NAVAL POSTGRADUATE SCHOOL

MONTEREY, CALIFORNIA

THESIS

INLET MASS FLOW MODELING AND MEASUREMENT THROUGH A TRANSONIC AXIAL COMPRESSOR FAN

by

Jay M. Wallen

June 2020

Thesis Advisor: Anthony J. Gannon
Co-Advisor: Walter Smith

Approved for public release. Distribution is unlimited.

THIS PAGE INTENTIONALLY LEFT BLANK

REPORT DOCUMENTATION PAGE	Form Approved OMB No. 0704-0188

Public reporting burden for this collection of information is estimated to average 1 hour per response, including the time for reviewing instruction, searching existing data sources, gathering and maintaining the data needed, and completing and reviewing the collection of information. Send comments regarding this burden estimate or any other aspect of this collection of information, including suggestions for reducing this burden, to Washington headquarters Services, Directorate for Information Operations and Reports, 1215 Jefferson Davis Highway, Suite 1204, Arlington, VA 22202-4302, and to the Office of Management and Budget, Paperwork Reduction Project (0704-0188) Washington, DC, 20503.

1. AGENCY USE ONLY *(Leave blank)*	2. REPORT DATE June 2020	3. REPORT TYPE AND DATES COVERED Master's thesis

4. TITLE AND SUBTITLE INLET MASS FLOW MODELING AND MEASUREMENT THROUGH A TRANSONIC AXIAL COMPRESSOR FAN	5. FUNDING NUMBERS
6. AUTHOR(S) Jay M. Wallen	
7. PERFORMING ORGANIZATION NAME(S) AND ADDRESS(ES) Naval Postgraduate School Monterey, CA 93943-5000	8. PERFORMING ORGANIZATION REPORT NUMBER
9. SPONSORING / MONITORING AGENCY NAME(S) AND ADDRESS(ES) N/A	10. SPONSORING / MONITORING AGENCY REPORT NUMBER

11. SUPPLEMENTARY NOTES The views expressed in this thesis are those of the author and do not reflect the official policy or position of the Department of Defense or the U.S. Government.

12a. DISTRIBUTION / AVAILABILITY STATEMENT Approved for public release. Distribution is unlimited.	12b. DISTRIBUTION CODE A

13. ABSTRACT (maximum 200 words)

This study investigated the creation of a 3-D computational fluid dynamics model of the Transonic Compressor Rig used for the testing of the Naval Postgraduate School Military Fan. This modeled rig conditions the flow into the rotor while measuring the mass flow rate during experimental testing. Using these simulations, a new bell mouth inlet attachment was designed for the rig to further increase confidence in experimental mass flow data. The goal of computational modeling was to observe upstream flow conditions and validate the model against experimental results, while also providing data for further testing. Also documented in this thesis is the performance data from the smooth casing rotor-only tests. All testing was performed at the Turbopropulsion Laboratory at the Naval Postgraduate School.

The bell mouth attachment design process included the evaluation of shape and diameter sizing for the desired pressure readings. The computational model was created using compressible flow turbulence modeling and run for various pressure differentials. A parametric study on throttle indexing was created by imitating the throttle's opening through the manipulation of the model's geometry. Results gave insight into upstream characteristics of the flow prior to the compressor, while also showing promising comparisons to recorded test data.

Future work will involve the inclusion of the bell mouth attachment in both testing and analytical simulation.

14. SUBJECT TERMS transonic rotor, axial compressor, CFD, mass flow rate measurement, bell mouth	15. NUMBER OF PAGES 97
	16. PRICE CODE

17. SECURITY CLASSIFICATION OF REPORT	18. SECURITY CLASSIFICATION OF THIS PAGE	19. SECURITY CLASSIFICATION OF ABSTRACT	20. LIMITATION OF ABSTRACT
Unclassified	Unclassified	Unclassified	UU

NSN 7540-01-280-5500

Standard Form 298 (Rev. 2-89)
Prescribed by ANSI Std. 239-18

THIS PAGE INTENTIONALLY LEFT BLANK

Approved for public release. Distribution is unlimited.

INLET MASS FLOW MODELING AND MEASUREMENT THROUGH A TRANSONIC AXIAL COMPRESSOR FAN

Jay M. Wallen
Ensign, United States Navy
BS, United States Naval Academy, 2019

Submitted in partial fulfillment of the
requirements for the degree of

MASTER OF SCIENCE IN ENGINEERING SCIENCE
(AEROSPACE ENGINEERING)

from the

NAVAL POSTGRADUATE SCHOOL
June 2020

Approved by: Anthony J. Gannon
Advisor

Walter Smith
Co-Advisor

Garth V. Hobson
Chair, Department of Mechanical and Aerospace Engineering

THIS PAGE INTENTIONALLY LEFT BLANK

ABSTRACT

This study investigated the creation of a 3-D computational fluid dynamics model of the Transonic Compressor Rig used for the testing of the Naval Postgraduate School Military Fan. This modeled rig conditions the flow into the rotor while measuring the mass flow rate during experimental testing. Using these simulations, a new bell mouth inlet attachment was designed for the rig to further increase confidence in experimental mass flow data. The goal of computational modeling was to observe upstream flow conditions and validate the model against experimental results, while also providing data for further testing. Also documented in this thesis is the performance data from the smooth casing rotor-only tests. All testing was performed at the Turbopropulsion Laboratory at the Naval Postgraduate School.

The bell mouth attachment design process included the evaluation of shape and diameter sizing for the desired pressure readings. The computational model was created using compressible flow turbulence modeling and run for various pressure differentials. A parametric study on throttle indexing was created by imitating the throttle's opening through the manipulation of the model's geometry. Results gave insight into upstream characteristics of the flow prior to the compressor, while also showing promising comparisons to recorded test data.

Future work will involve the inclusion of the bell mouth attachment in both testing and analytical simulation.

THIS PAGE INTENTIONALLY LEFT BLANK

TABLE OF CONTENTS

I. INTRODUCTION 1
- A. MOTIVATION 1
- B. THESIS OBJECTIVES 2

II. BACKGROUND INFORMATION 3
- A. PREVIOUS WORK 3
- B. MASS FLOW MEASUREMENT 4
- C. BELL MOUTH DESIGN 5

III. DESIGN 7
- A. CURRENT SETUP 7
- B. DESIGN REQUIREMENTS 10
- C. CYLINDER CASING 10
- D. BELL MOUTH ATTACHMENT 11
- E. SUPPORTS 14

IV. COMPUTATIONAL FLUID DYNAMICS ANALYSIS 15
- A. 60 DEGREE WEDGE MODEL 15
- B. THROTTLE LEVEL MODELING 16
- C. ANSYS CFX SETUP 18
  - 1. Geometry and Design Modeler 18
  - 2. Mesh 19
  - 3. CFX-Pre Setup 22
  - 4. Solution Controls 25
  - 5. Parameterization 25
- D. FLOW SCREEN MODELING EXPLORATION 26
- E. SIMULATION RESULTS 29
  - 1. High Pressure Issues 29
  - 2. Mass Flow Rates and Mach Numbers 29
  - 3. Pressure Profiles at Measurement Locations 33
  - 4. Turbulent Kinetic Energy Profiles 36

V. EXPERIMENTAL RESULTS 39
- A. DATA RUNS SETUP 39
- B. PERFORMANCE CURVES AND EFFICIENCIES FOR NPSMF 40

VI. CONCLUSION 43
A. SUMMARY 43
B. RECOMMENDATIONS FOR FUTURE WORK.....43

APPENDIX A. ASME MFC-26-2011 BELL MOUTH INLET FLOWMETERS GUIDELINES 45

APPENDIX B. BLAIR AND CAHOON BELL MOUTH DESIGN 47

APPENDIX C. CYLINDRICAL CASING DRAWINGS 51

APPENDIX D. BELL MOUTH COMPRESSIBLE FLOW CALCULATION.....55

APPENDIX E. MACHINED BELL MOUTH ATTACHMENT DRAWINGS.....57

APPENDIX F. CFX MODEL MESH STATISTICS.....63

APPENDIX G. KEY CFD SIMULATION RESULTS 67

APPENDIX H. PERFORMANCE CURVES FOR NPSMF.....69

APPENDIX I. MASS-AVERAGED EFFICIENCY CURVES FOR NPSMF 71

APPENDIX J. ADDITIONAL TCR AND BELL MOUTH ATTACHMENT VIEWS 73

APPENDIX K. PRESSURE DROP ACROSS TCR COMPARISON 75

SUPPLEMENTAL. EXPERIMENTAL RAW DATA FILE.....77

LIST OF REFERENCES.....79

INITIAL DISTRIBUTION LIST 81

LIST OF FIGURES

Figure 1. 18 degree wedge geometry of single rotor blade and fluid. Source: [5]. 4

Figure 2. Velocity flow profiles into a bell mouth pipe. Source: [8]. 6

Figure 3. TCR throttle component disconnected from rig. 8

Figure 4. Representation of the throttle's two-plate rotation method. 8

Figure 5. TCR final rotor stage engineering drawing. Source: [5]....9

Figure 6. Isometric views of cylindrical casing. 11

Figure 7. Basic sketch of elliptical profile bell mouth shape. 12

Figure 8. Compressible flow calculation results for varying bell mouth exit diameters. 13

Figure 9. Isometric views of machined bell mouth attachment. 14

Figure 10. 60 degree wedge model of the flow through the TCR. 16

Figure 11. Flow-line view of rotated front body to imitate a throttle level. 17

Figure 12. Isometric view of rotated throttle setting. 17

Figure 13. Design Modeler tree outline and rotation details. 19

Figure 14. Mesh around throttle near inlet of TCR. 20

Figure 15. Mesh around mass flow nozzle. 21

Figure 16. Full mesh of TCR. 21

Figure 17. CFX-Pre outline with all defined boundaries and interfaces. 23

Figure 18. CFX-Pre setup applied to TCR model. 24

Figure 19. Interrupt control expression used in CFX runs. 25

Figure 20. Geometry of TCR model with two flow screens included. 26

Figure 21. Coarse mesh of TCR model with included flow screens. 27

Figure 22. CFX-Pre setup settings for the flow screens included in some model runs. 28

Figure 23. Mass flow rate curves derived from CFD flow analysis. 30

Figure 24. Mach number profile for 10 kPa and an open throttle. 31

Figure 25. Mach number profile for 25 kPa and 12.273 degree rotated throttle (50% covered). 32

Figure 26. Stagnation and static pressure curve locations. 34

Figure 27. Stagnation pressure profile over the length of the stagnation pressure curve from CFD simulation. 35

Figure 28. Static pressure profile over the length of the static pressure curve from CFD simulation. 36

Figure 29. Turbulent kinetic energy color map at the nozzle exit plane. 37

Figure 30. Turbulent kinetic energy profile over the vertical distance from the wedge tip to the wall of the model. 38

Figure 31. T-s diagram for TCR and NPSMF operation. 39

Figure 32. Performance curve of NPSMF at 70% speed +/- 1σ. 40

Figure 33. Overlay of performance curves from experimental data and mass flow rate curves from CFD analysis. 41

Figure 34. Mass averaged efficiency of NPSMF at 70% +/- 1σ. 42

Figure 35. Three bell mouth shapes tested by Blair and Cahoon [8]. 47

Figure 36. C_D improvements for each bell mouth shape tested by Blair and Cahoon [8]. 48

Figure 37. Mass flow rate improvements for each bell mouth shape tested by Blair and Cahoon [8]. 48

Figure 38. Pressure drop across the TCR for a matched 70% speed experimental test. 73

LIST OF TABLES

Table 1. Degrees of rotation used to model throttle percentages. 18

Table 2. Mesh statistics for full TCR 22

THIS PAGE INTENTIONALLY LEFT BLANK

LIST OF ACRONYMS AND ABBREVIATIONS

ANSYS CFX	A commercial CFD code
CFD	Computational fluid dynamics
C_D	Discharge coefficient
NPS	Naval Postgraduate School
NPSMF	Naval Postgraduate School military fan
TCR	Transonic compressor rig
TPL	Turbopropulsion laboratory

THIS PAGE INTENTIONALLY LEFT BLANK

ACKNOWLEDGMENTS

Many thanks to Dr. Hobson, Dr. Gannon, and Dr. Smith for introducing me to the process of turbomachinery testing as well as the commercial design process with machinists. Their insight into flow analysis and the use of CFX was invaluable to producing this thesis, and it saved me many hours of frustration. I also thank all the staff at NPS TPL for allowing this research to happen even in the midst of very unique times of sheltering in place.

THIS PAGE INTENTIONALLY LEFT BLANK

I. INTRODUCTION

A. MOTIVATION

The shaping and constructing of a specific flow with desired boundary conditions in a repeatable fashion requires significant precision and attention to detail. Such precision and detail is also of utmost importance in the testing of advanced turbomachinery and the analysis of its performance. This study pursued this work for the testing of a transonic compressor rotor known as the Naval Postgraduate School Military Fan (NPSMF). The Naval Postgraduate School (NPS) has been testing the NPSMF at the Turbopropulsion Laboratory (TPL) in order to accurately determine its performance characteristics at various operating conditions. The NPSMF is being tested within the TPL's transonic compressor rig (TCR)—a rig that requires around 9.144 meters (30 feet) of pipes and nozzles devoted to straightening and measuring the exact characteristics of the flow when it reaches the rotor's face.

In particular, the mass flow rate entering the NPSMF must be measured to be used in calculations of the fan's performance. To ensure that these experimental measurements are accurate, the mass flow rate must be measured at multiple locations in multiple manners. The current mass flow rate measurement system within the TCR is not optimal, particularly with respect to ensuring proper boundary conditions for these measurements. This system also provides non-ideal inflow conditions to the test article, disturbing the flow in an undesirable manner. Providing redundancy in the mass flow rate measurements and including more consistent methods will increase the fidelity of the experimental performance data. In order to achieve this, a new bell mouth inlet attachment needed to be designed for the TCR to provide accurate, consistent boundary conditions for the recording of experimental data.

The well characterized nature of a bell mouth inlet would also provide the correct conditions for computational modeling of the flow. Current computational fluid dynamics (CFD) models of the TCR disagree with the experimental data, revealing the need for a more accurate analytical model. Such a model would provide significant insight into the

nature of the flow throughout the rig and allow for additional research into the effects of adjustments to the rig on the flow characteristics entering the test rotor. Both a detailed CFD model of the full TCR and an additional bell mouth attachment for mass flow rate measurement would significantly benefit performance research for the NPSMF.

B. THESIS OBJECTIVES

The research in this thesis centered on experimental mass flow rate measurement guidelines for the TCR and bell mouth design practices to achieve consistent boundary conditions at the TCR's inlet. Design work involved the modeling of the bell mouth attachment and the required cylinder casing surrounding the TCR's throttle using Solidworks. The bulk of the thesis focused on the CFD modeling of the full TCR using ANSYS Workbench and CFX fluid simulation. The thesis also included an analysis of the CFD results at various throttle positions and various levels of additional detail. Finally, this thesis documented the performance data for the NPSMF at smooth casing operation and validated the CFD model's results with this data.

II. BACKGROUND INFORMATION

A. PREVIOUS WORK

Research on transonic compressors in the TCR has been ongoing for many years, with data continuing to be taken and different aspects of rotors being analyzed. Initial work was undertaken by Villescas, 2005 [1], who completed three-hole probe flow field surveys of the compressor rotor. These probes measured the static and stagnation pressures within the free stream jet and were calibrated in order to be used in the TCR to determine the magnitude and direction of the flow by rotation in the field. This method aimed to experimentally determine the flow into the rotor and its performance characteristics.

Brunner [2] then completed 5-probe surveys and used CFD to model the rotor and analyze the flow computationally. The experimental data was compared to the 3-probe surveys. ANSYS CFX was used to make numerical predictions of the flow, which were then compared to the experimental data. These were only the most basic simulations of the inlet duct.

In late 2005, Payne [3] followed in the probe survey and CFD work, but applied it to the rotor during steam-ingestion, focusing on performance prior to and during a steam-induced stall. He also experimentally focused on the kinetic turbulence intensity at the compressor at the various operating speeds.

Koessler [4] directed a study towards the stall of the rotor, but included work in mass flow rate measurement in 2007. These were the initial stages of mass flow rate measurement and verification, using total temperature and pressure from the inlet to compare to the readings taken at the rotor face. This setup is still used, although it has been refined and improved upon with newly manufactured parts.

The most direct relation to this research concluded in 2019 in work done by Thorton [5]. He sought to improve the computational-modeling fidelity of the NPSMF by modeling the rotor blade in ANSYS Mechanical and coupling it with a CFX fluid simulation. In order to do this, he had to model fluid-structure interactions by integrating two separate geometries into the ANSYS Workbench. He then compared the computational results to

the experimental results to ensure its accuracy. By doing so, he sought to be able to predict the performance of other transonic-rotor geometries without the high cost of running the TCR repeatedly for experimentation. Thorton [5] implemented his model using an 18 degree slice of the flow pipe to match the 18 degree slice of test section previous created by McNab [6], covering only the flow that would pass over and be affected by a single rotor blade. The coupled wedge used can be seen in Figure 1.

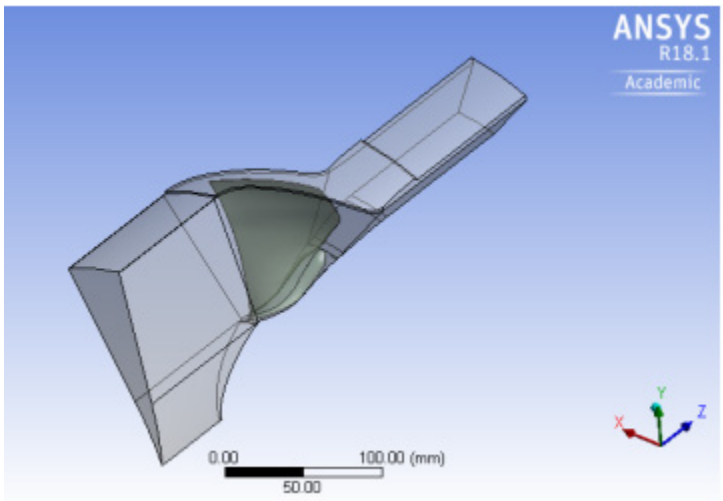

Figure 1. 18 degree wedge geometry of single rotor blade and fluid. Source: [5].

This method cut down on computational time significantly, while being adjusted appropriately to relate to experimental data. A similar method was modified and used for this research, altered to include all necessary components of the TCR. Thorton [5] applied the method to the flow nozzle in the rig upstream of the NPSMF and the internal bell mouth slightly farther upstream to begin observing the flow as it leads to the compressor and to determine its characteristics. This thesis further extended this model to the entire TCR from inlet to compressor face.

B. MASS FLOW MEASUREMENT

The simplest and most prevalent way mass flow rates are measured within turbomachinery is through the use of pressure measurements. Devices measure the static

pressure at various points in the rig and use those values along with the stagnation temperature and pressure of the inlet air to calculate the mass flow rate. For compressible flow, the stagnation velocity, a non-dimensionalized velocity "X," is calculated using these pressures, and the ideal mass flow rate is found using that stagnation velocity and assuming a constant velocity and density profile at the exit plane.

$$X = \frac{v}{v_o} = \sqrt{1 - \left(\frac{P_1}{P_{t1}}\right)^{\frac{\gamma-1}{\gamma}}}$$

$$\dot{m}_{ideal} = (1 - X^2)^{\frac{1}{\gamma-1}} X A \frac{P_{t1}}{R} \sqrt{\frac{2C_p}{T_{t1}}}$$

This ideal mass flow rate is then related to the experimental mass flow rate by the discharge coefficient (C_D) for the given rig. This discharge coefficient is the ratio of the two mass flow rates.

$$C_D = \frac{\dot{m}_{exp}}{\dot{m}_{ideal}}$$

Mass flow rate measurements are often taken through the use of a bell mouth inlet for turbomachinery applications, as these inlets are efficient and have discharge coefficients close to unity. ASME MFC-26-2011 [7] is the standard for the measurement of gas flow by bell mouth flowmeters, and details on its guidelines and parameters are found in Appendix A.

C. BELL MOUTH DESIGN

A bell mouth inlet provides a reliable geometry by which one can measure the mass flow into a pipe, making it an excellent choice for an additional measurement system within the TCR. Such measurement methods have been widely documented and best practices proven. For the purposes of this research, the bell mouth design required a high efficiency with a discharge coefficient close to unity for minimal necessary correction to the mass flow data. Measurements closer to ideal flow rates would also provide increased confidence in their accuracy.

The exact parameters of a bell mouth's shape determine its efficiency in operation. It was of great importance to ensure the design characteristics of the bell mouth were well documented and that the final geometry was constructed as closely as possible to the design intent. This would ensure the proper conditions used in measuring the mass flow rates. Considerations for the bell mouth's design include ratio of diameters, profile shape, and radial tip size. A study by Blair and Cahoon [8] simulated a large number of different sizes and profiles of bell mouth to determine the most efficient configuration. Their conclusion was that an elliptical profile outperformed all other bell mouth shapes to provide the most ideal mass flow rate values and efficient discharge coefficients. Their study included computational model simulations like the one shown in Figure 2. Design work in this thesis relies on this study as its basis. Further details of the study are available in Appendix B.

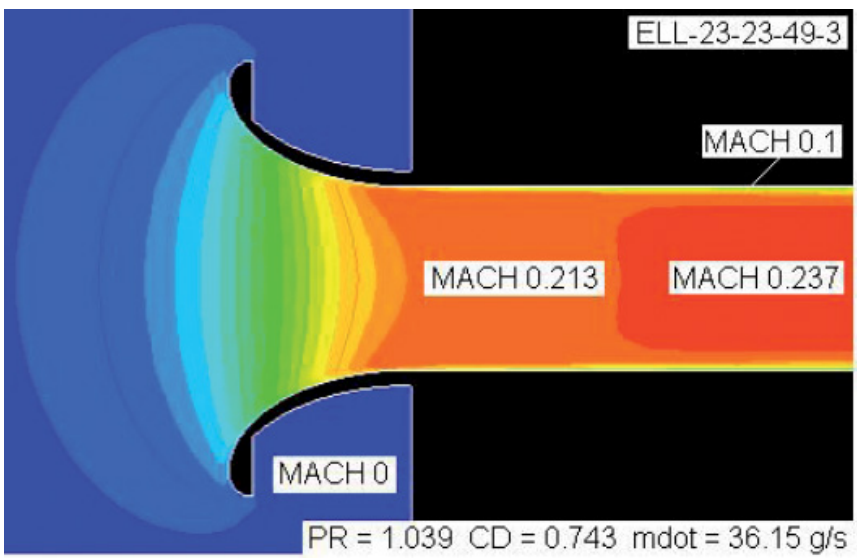

Figure 2. Velocity flow profiles into a bell mouth pipe. Source: [8].

III. DESIGN

The TCR has been used to test various pieces of turbomachinery over many years of operation, as the previous theses listed demonstrate. As various rotors have cycled through the test rig, the rig itself has grown and improved to allow for more diverse measurement methods, shorter sampling times, and more accurate results. The design of this additional attachment had to match the already present configuration and maintain the existing features used in testing.

A. CURRENT SETUP

The existing rig includes a box inlet opening up to outside air. This inlet includes a screen to prevent the ingestion of any foreign objects into the rig. It is a basic setup that provides no means of flow measurement and limited boundary condition settings.

Within this box is the TCR throttle – a cylindrical-shaped piece with 6 sets of three-holed inlets, shown in Figure 3. The throttle contains another circular plate behind the front plate with an identical hole pattern. The rotation of the second plate to various degrees closes the throttle, adjusting the speed of inflow to the testing rotor. Figure 4 shows a mockup image of the throttle's rotation mechanism. The throttle is marked with 12 valve positions but can be adjusted anywhere between graduations. The operating range of the system rarely covers more than around half of that marked range, and test settings vary depending on the compressor being tested. For the NPSMF, typical valve positions range between 1 and 6.3, increasing by successively smaller increments as the compressor approaches stall. The positions are viewed through a window in the outer inlet box, and this operational necessity must be preserved. Additionally, multiple wires exit the outer inlet box towards the back bottom right corner which control the throttle and provide measurement readings at the inlet plane. These also must be accounted for in the new design.

Figure 3. TCR throttle component disconnected from rig.

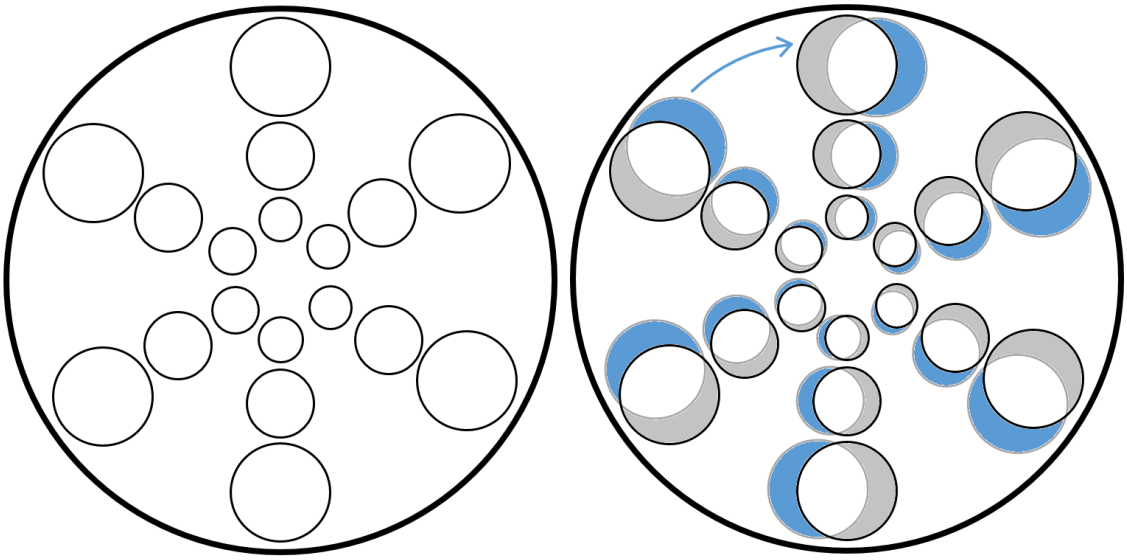

Figure 4. Representation of the throttle's two-plate rotation method.

The throttle then leads into the main piping of the TCR, where flow passes through a flow-straightening screen and then through a thicker hexagonal screen to remove any induced swirling of the flow. At the end of this long pipe section, the flow accelerates through an interior bell mouth shape, followed by a mass flow measurement nozzle. This interior nozzle has been used up to this point to measure the mass flow rate in the TCR using pressure and temperature probes, and the overall discharge coefficient used for the rig was derived from these measurements. This C_D value of 1.03 has been investigated through the use of CFD analysis by Thorton [5] referenced earlier. The higher than unity value has been determined to be a result of flow recirculation regions in the non-optimal installation configuration.

After the mass flow nozzle, the piping continues into a final pre-rotor bell mouth that uses pressure taps and probes to measure flow characteristics directly prior to the operating rotor's face. The final rotor stage can be seen in Figure 5.

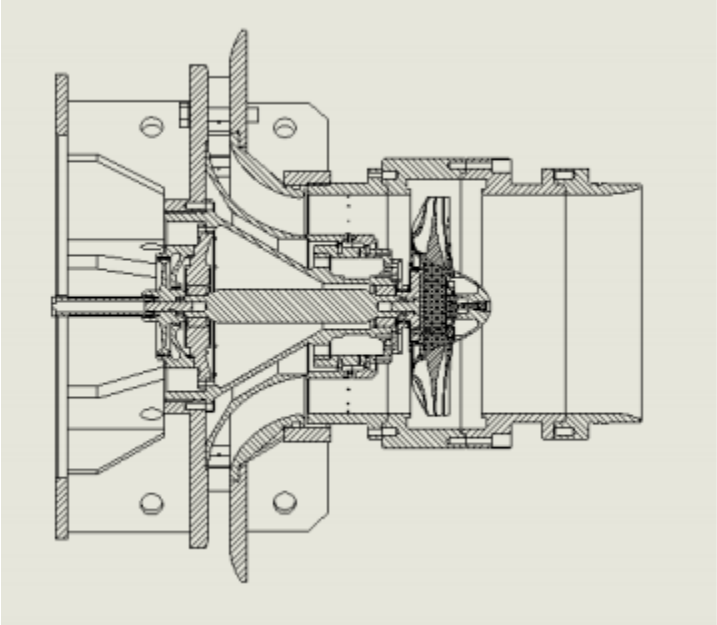

Figure 5. TCR final rotor stage engineering drawing. Source: [5].

B. DESIGN REQUIREMENTS

The bell mouth attachment design was intended to replace the box inlet entirely, and thus had to fit around the throttle and include the referenced features for operation. This includes the throttle level indicator and the electrical outlet wires. The new design also needed to include an additional outlet hole for the humidity measurement device that had been placed at the exterior screen of the box inlet. The bell mouth inlet needed to align with the ideal mass flow measurement guidelines outlined in ASME MFC-26-2011 [7]. This included a length of constant diameter pipe that stretched at least one diameter away from the bell mouth's exit in order to ensure that the pressure probes can take measurements of the flow after it has fully developed. The bell mouth also needed to be properly sized in order to have a sufficiently large pressure differential of 3 kPa for the implemented probes and for desired mass flow rates of 6–10 kg/s.

After the end of the bell mouth's constant diameter section, the attachment then needed to expand in diameter to fully encompass the throttle. This conical connection can be seen in the next section in Figure 6 as a part of the cylinder casing. The entire interior of the attachment needed to be machined smoothly enough to not trip or disrupt the flow in any way leading down the pipe. The expansion section also needed to be smooth and ensure that it did not trip the flow into becoming turbulent or cause any undesirable movement entering the throttle. Once through the throttle, the flow would follow the path explained above. Finally, the entire setup would require a support structure that could easily move the large piece to attach or remove it from the TCR depending on the desired testing parameters. This motion had to be possible on uneven tarmac on which the exit of the TCR rests.

C. CYLINDER CASING

The simpler section to design was the casing around the throttle. The most efficient method of covering the throttle without excess weight or areas of backflow is a cylindrical casing. The cylinder's is required to be at least 1.219 meters (48 inches) in internal diameter to encompass the throttle and allow for the level readings to be seen through a window cut into the upper portion. This window would be covered with a clear plastic covering that

must be sealed to prevent airflow from escaping. The transition to the smaller bell mouth diameter is accommodated by a conical connector piece that must be bolted to the bell mouth attachment by internal flanges. These internal flanges allow for much easier machining of the part, and they provide a backwards facing step for the flow entering the cylindrical chamber, ensuring a steady flow. The entire casing is constructed out of stainless steel 3.175e-3 meters (1/8") thick to allow for minimal material requirements with maximum strength as well as protection from corrosion. The Solidworks 3-D model can be seen in Figure 6. The full drawings in detail can be found in Appendix C.

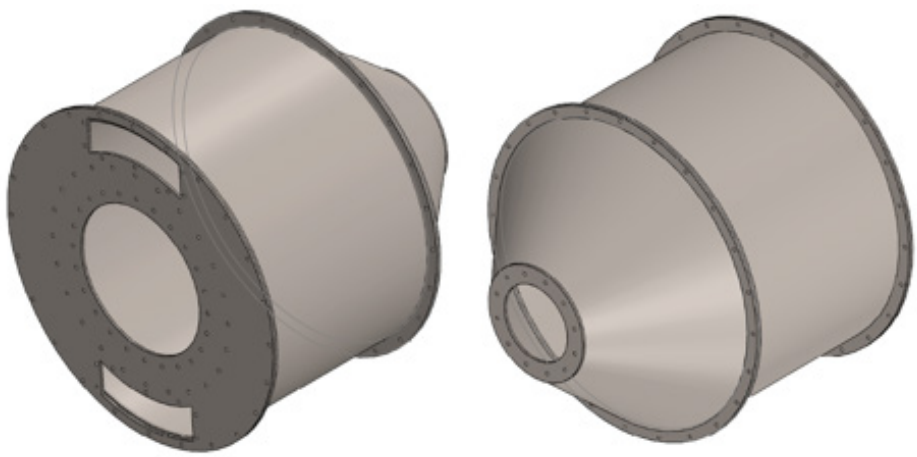

Figure 6. Isometric views of cylindrical casing.

D. BELL MOUTH ATTACHMENT

The bell mouth portion of the attachment, as explained previously, had to be sized properly to align with the ASME standard, the bell mouth design guidance for optimum efficiency, and the pressure differential and mass flow rate requirements of the planned tests. Blair and Cahoon [8] proved an elliptical bell mouth shape to be the most efficient. The sketch shown in Figure 7 outlines the ellipse profile shape.

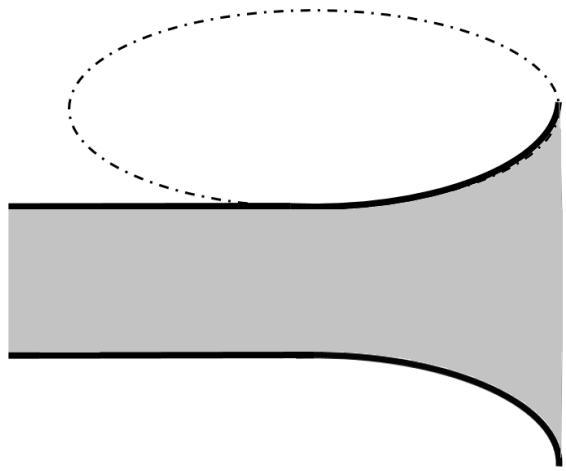

Figure 7. Basic sketch of elliptical profile bell mouth shape.

The outer diameter was determined by estimating the flow into the bell mouth at various diameters by using compressible flow calculations. The mass flow rate was varied between the 6 kg/s and 10 kg/s while the static and stagnation pressure ratio was varied between 0.95 and 0.99. Using stagnation velocity and the derived compressible density and velocity expounded upon previously, the areas required were found. The calculations used and the table formulated can be found in Appendix D, while the results can be seen plotted in Figure 8. Based on these results and in order to ensure an accurately measureable pressure ratio of at most 0.975, a bell mouth exit diameter of 0.3048 meters (12 inches) was determined to be appropriate.

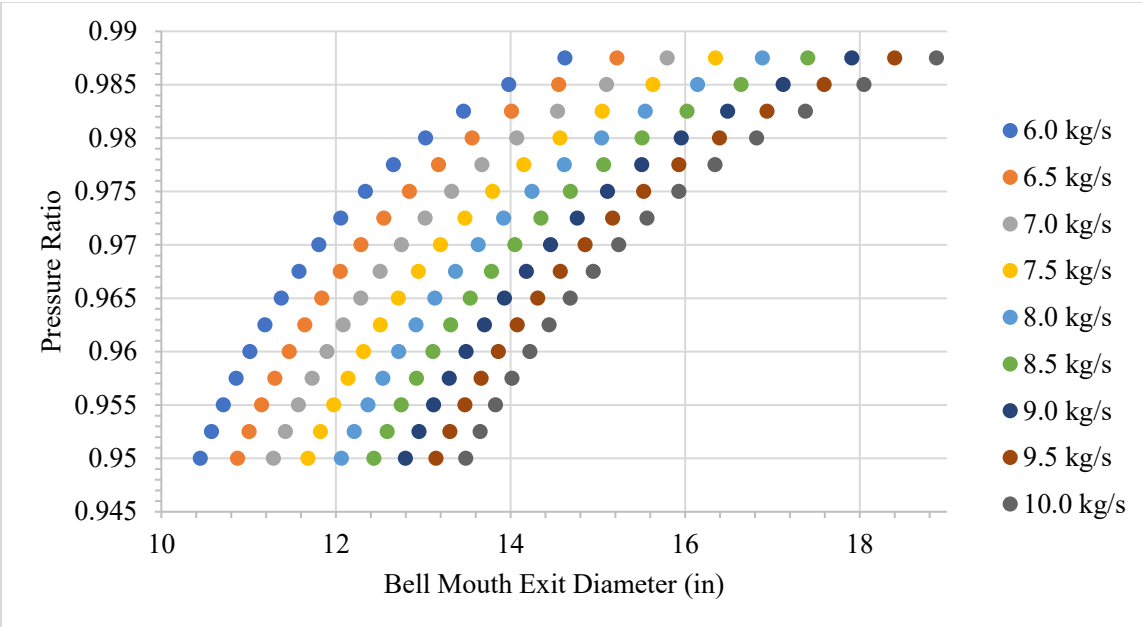

Figure 8. Compressible flow calculation results for varying bell mouth exit diameters.

With the bell mouth exit size determined, Blair and Cahoon [8] guidance advised a short and stocky bell mouth for the most ideal discharge coefficients, leading to the decision to make the elliptical profile 0.3048 meters (12 inches) and 0.1016 meters (4 inches) in radii. The length of constant diameter tubing following the bell mouth extends out to 0.3937 meters (15.5 inches) past the bell mouth's exit in order to provide substantially enough distance for the flow to settle prior to pressure measurements being taken.

The bell mouth is constructed out of 6061 aluminum because it is easier to machine and this portion of the attachment requires less strength than the cylinder casing. In order to make it simpler to machine, it was divided into four sections that would be bolted together. These pieces would include press-fit sealing by means of 5.08e-5 meter (0.002 inch) gaps between bolt flanges. The piece closest to the conical link of the cylindrical casing houses the four pressure tap locations for mass flow measurement. The full design drawings can be found in Appendix E. The 3-D Solidworks model can be seen in Figure 9.

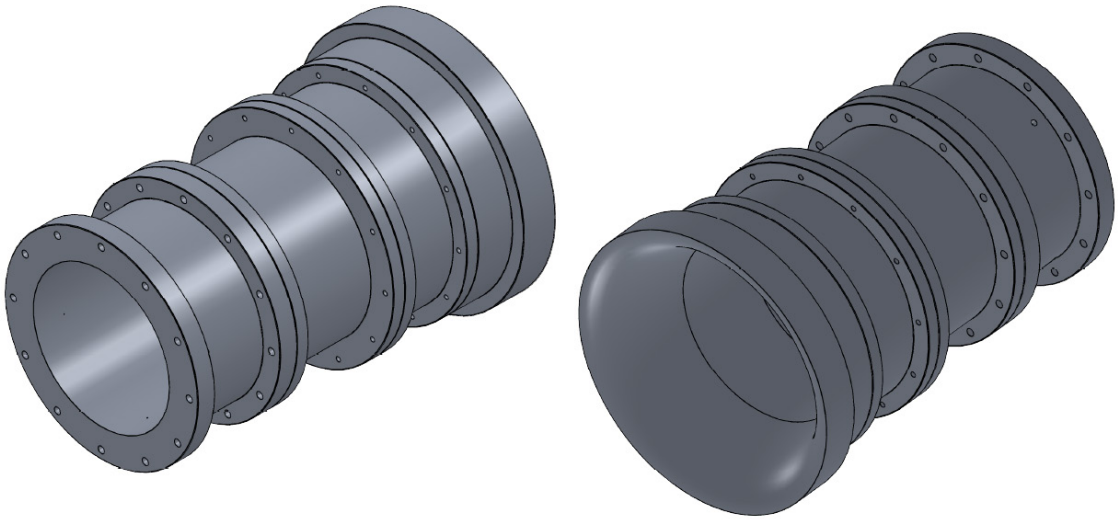

Figure 9. Isometric views of machined bell mouth attachment.

E. SUPPORTS

The final design process involved the support structure for the entire attachment. The attachment's final weight was 235.98 kg (520.24 lbs), and its center of mass resided around the center of the conical link. Due to the cylindrical portion's large diameter, the attachment leaves only around 0.3302 meters (13 inches) of clearance with the ground when attached. For this reason, and for the sake of stability, the supports were designed to attach on the side of the cylindrical section. In order to accommodate the forward center of mass, another connection was designed to extend up to the central portion of the bell mouth attachment. Industrial casters were used to ensure that the entire attachment can be rolled off the TCR and out of the way of incoming flow if necessary.

IV. COMPUTATIONAL FLUID DYNAMICS ANALYSIS

Apart from the Solidworks design process of the bell mouth attachment, the remaining bulk of research was centered on the CFD model of the entire TCR. A full model of the rig had to this point never been created, and the process required the inclusion and consideration of many detailed attributes. This model included all sections of the TCR: the box inlet, throttle, interior bell mouth, mass flow nozzle, and pre-rotor bell mouth. Initial set up did not include the bell mouth attachment. This addition will be incorporated in later work.

A. 60 DEGREE WEDGE MODEL

Building off of previous work by Thorton [5], the TCR was modeled as a wedge representing a fraction of the circular piping. Thorton [5] used an 18 degree model of the flow directly around a rotor blade and also modeled a 1.8 degree partial section of the upstream rig to reduce computational time further. The section included only the mass flow nozzle and a section of piping allowing for the flow to full develop. When modeling the entire rig, the throttle necessitated a larger wedge to accurately model its geometry. The throttle, shown in Figure 4, contains six columns of three inlet holes. Thus the model required a 60 degree wedge with periodic sides to represent the motion of flow through one-sixth of the entire rig. This was created in Solidworks by outlining a perpendicular view of the rig from the center of the piping to the outer walls and then rotating it about the central axis 60 degrees. The model, shown in Figure 10, represents all areas of the flow within the TCR.

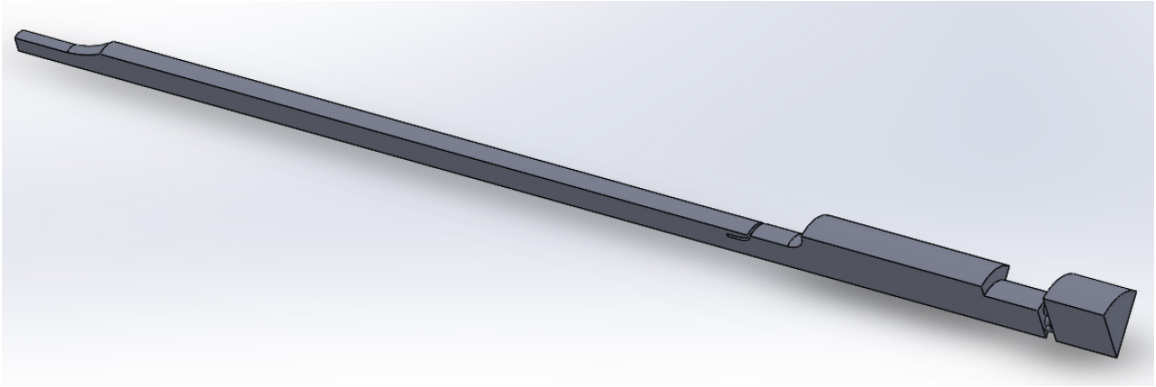

Figure 10. 60 degree wedge model of the flow through the TCR.

B. THROTTLE LEVEL MODELING

The throttle also required another modification to fully capture its various level settings. The throttle's levels are determined by the rotation of the plate residing directly behind the front surface. Because these two surfaces are exactly the same, their inlet holes could be modeled by splitting the CFD model down the middle of the throttle. This created two sets of holes representing the flow passing through each plate. The two resulting sections were connected in an assembly and could then be loaded into CFX as a parasolid containing two bodies. To model the different levels, then, one of the two bodies needed to be rotated along their common wedge axis. For the sake of ease, the front body was used as the rotated body. An example of the TCR model with a rotated throttle setting can be seen in Figures 11 and 12.

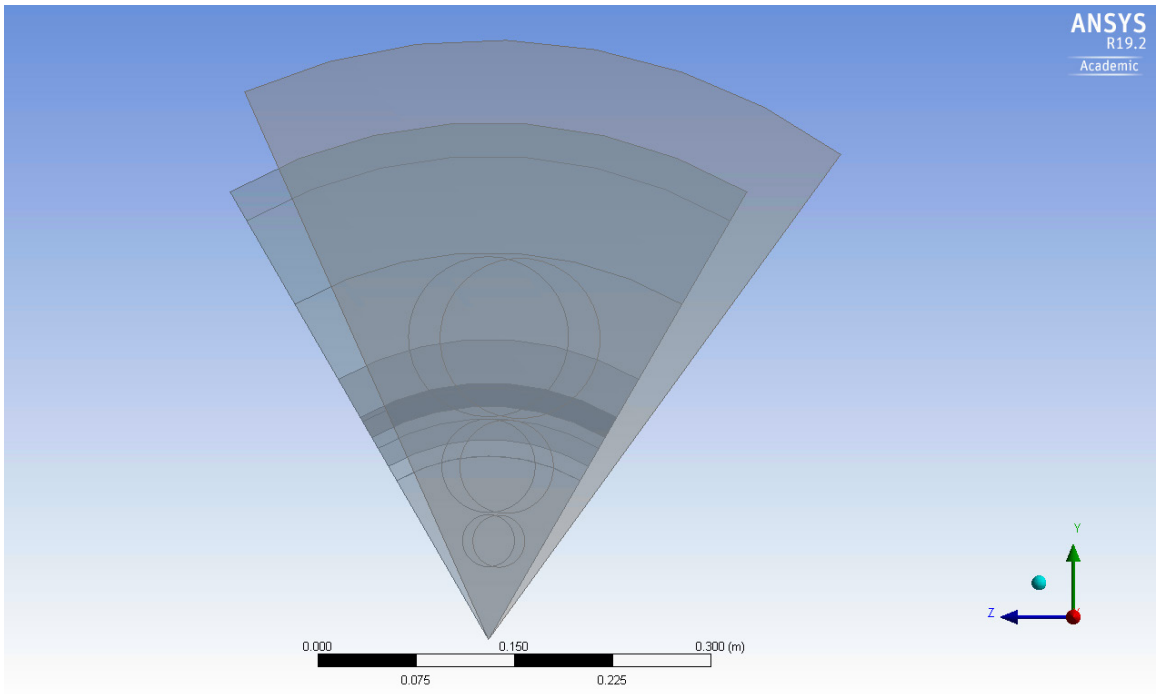

Figure 11. Flow-line view of rotated front body to imitate a throttle level.

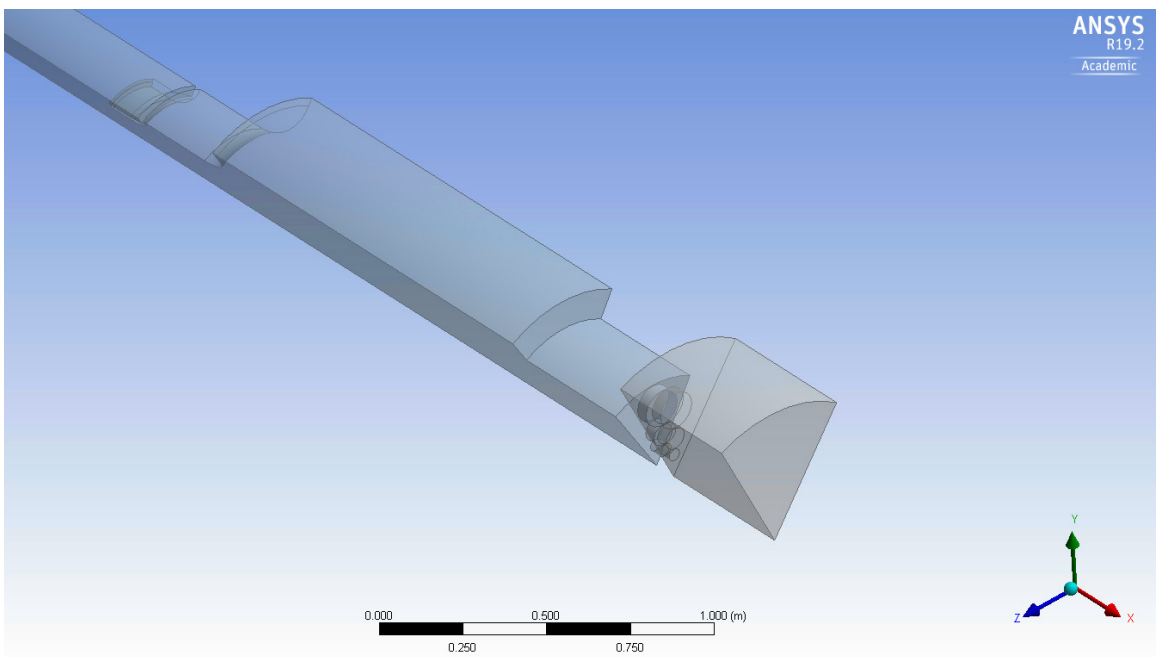

Figure 12. Isometric view of rotated throttle setting.

The next step was to determine how to quantify how much the throttle area was reduced with a given rotation. It was decided that the TCR would be initially analyzed at various percentages of covered throttle for reference, particularly at 25% covered, 50% covered, and 60% covered. In order to calculate the angle of rotation required for each percentage, the area of a lens created by two intersecting circles needed to be calculated. Assuming two circles of equal radius R, the resulting area of the lens can be found using the following equation.

$$A_{lens} = 2R^2 \cos^{-1}\left(\frac{d}{2R}\right) - \frac{d}{2}\sqrt{4R^2 - d^2}$$

where d = distance between the centers of the two circles

Setting the area A_{lens} equal to 75% of the area of one throttle circle and solving for d gives the distance between the centers of the throttle circles for a 25% covered throttle setting. The angle of rotation required to achieve that distance between centers can then be calculated using trigonometry. The angles used for each throttle level analyzed can be found in Table 1.

Table 1. Degrees of rotation used to model throttle percentages.

Percentage of Throttle Covered	Degrees of Rotation
25%	5.99559
50%	12.2725
60%	14.9564

C. ANSYS CFX SETUP

1. Geometry and Design Modeler

The parasolid assembly was inserted into a basic CFX block in ANSYS workbench, consisting of the front and back separated bodies. A rotation was then created under the "Insert" tab within Design Modeler for the smaller front body, with the axis defined as the

wedge convergence line. The rotation could then be adjusted by setting the angle of rotation to whatever degree was required for each throttle level, as specified previously. The Design Modeler outline with the inserted rotation can be seen in Figure 13.

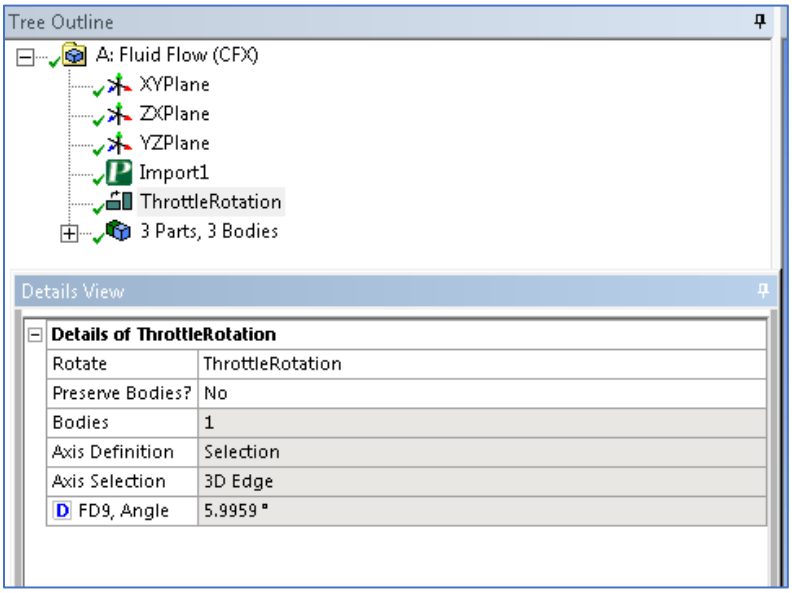

Figure 13. Design Modeler tree outline and rotation details.

2. Mesh

The mesh for this model took significant refinement in particular areas due to its complexity. The final mesh was also quite large due to the TCR's length from inlet to rotor. The goal for the bulk mesh was to provide a fine enough mesh to capture any possible flow swirling, separation zones, or other characteristics within the body of the wedge. As the meshing approached the walls, however, further refinement was necessary. A finer mesh closer to the walls was required to capture the full effects of recirculation and pressure effects at the corner intersections within the TCR. Additionally, this refinement was required to prevent too large of an aspect ratio between the bulk global mesh and the inflation layers up against the walls. These inflation layers were the last form of mesh refinement in order to reduce the y+ values throughout the rig, ensuring that the boundary layer flows were properly resolved. The y+ goals achieved were values of less than 10 in the mass flow nozzle and less than 10 averaged over the entire wall domain. The inflation

layers kept the maximum y+ along the wall domain around a value of 100. A thinner inflation layer was placed on the walls of the mass flow nozzle to ensure that the pressure and turbulent kinetic energy at those critically measured locations were accurate. Refinement sizing were placed around the walls of the throttle to ensure sufficiently detailed meshing in that area of flow acceleration and compression. A match control was set on either side of the wedge to ensure that the periodicity was correctly modeled without unnecessary interpolation. Some examples of the refined mesh locations can be seen in Figures 14 and 15. The full mesh can be seen in Figure 16.

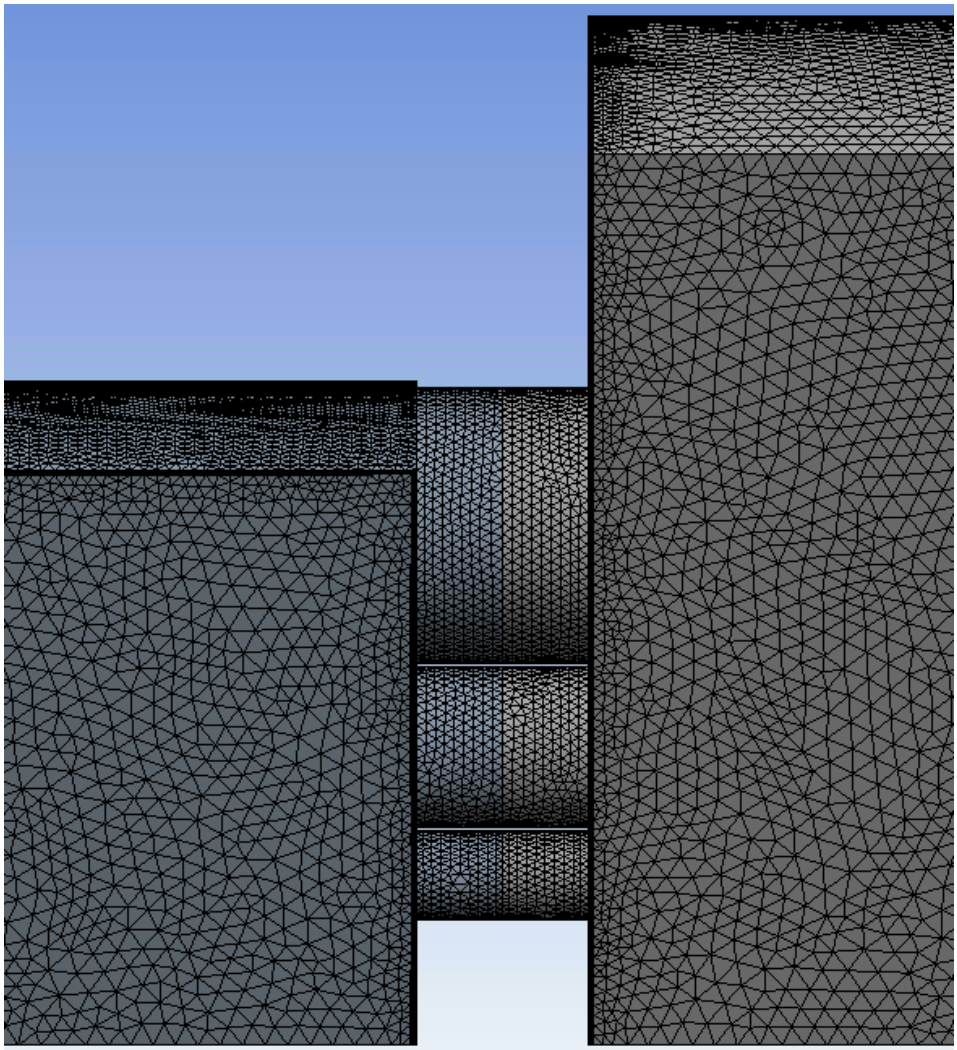

Figure 14. Mesh around throttle near inlet of TCR.

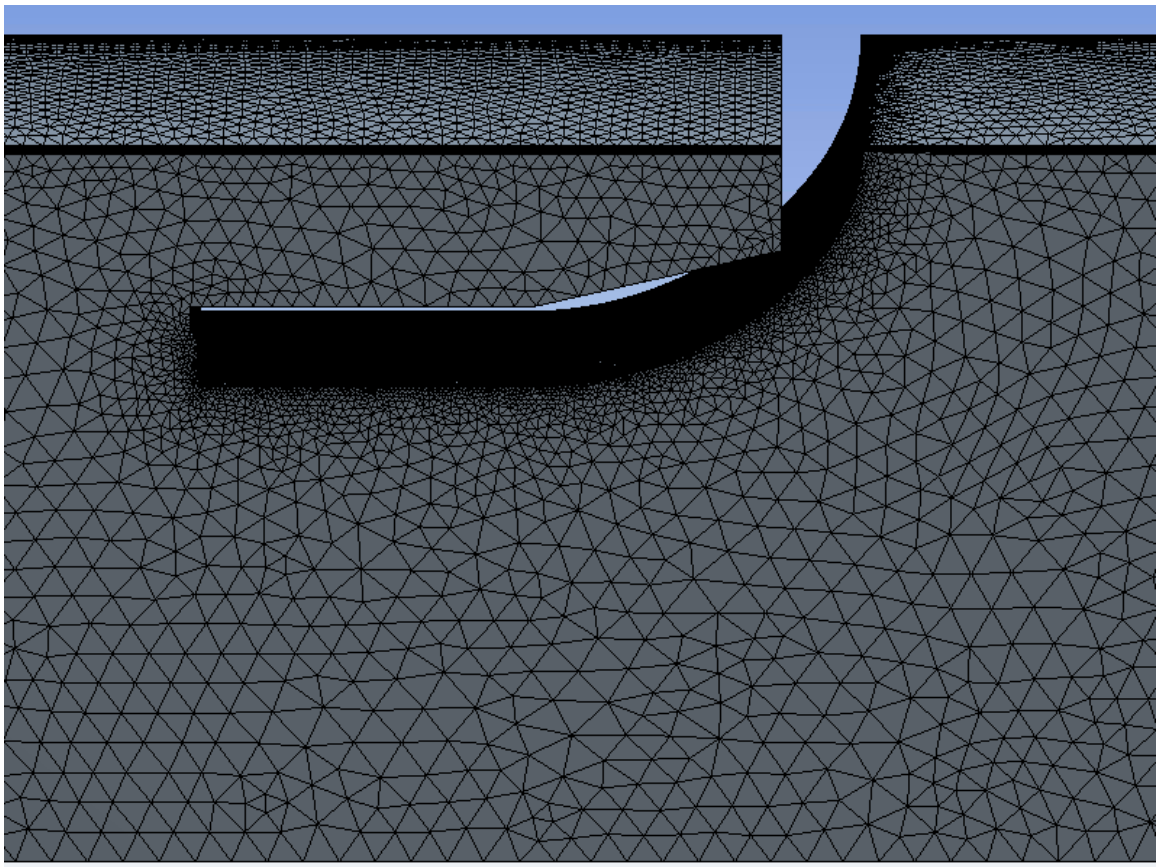

Figure 15. Mesh around mass flow nozzle.

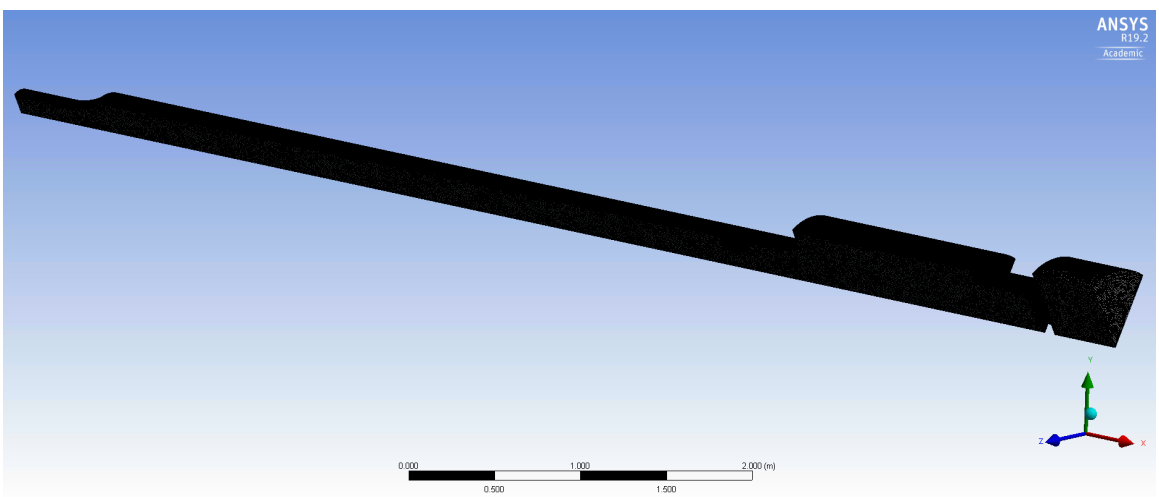

Figure 16. Full mesh of TCR.

Table 2 shows the mesh elements and nodes for the TCR. The full details of the mesh can be found in Appendix F.

Table 2. Mesh statistics for full TCR

Mesh Elements	8,135,034
Mesh Nodes	2,576,986

3. CFX-Pre Setup

Setup here required significant detail as well as trial and error to identify the adjustments required to ensure the CFX solver converged on an appropriate and accurate solution. For "Default Domain – Basic Settings," the "Fluid 1" material was set to "Air Ideal Gas," and the reference pressure set to 1 atm. The "Total Energy" heat transfer option was used under "Fluid Models," and the "Shear Stress Transport" turbulence model was used.

The inlet and outlet planes were defined in the typical manner as inlet and outlet boundaries. The inlet boundary was defined by a total pressure of 0 kPa with respect to the overarching relative pressure of 1 atmosphere. This represented the physical condition of atmospheric air at the box inlet. The total temperature was also defined in accordance to typical Monterey, California, weather, where NPS is located—approximately 285 K. The outlet boundary was defined by a relative static pressure, creating the pressure differential across the model to initiate flow.

Because the geometry of this model is designed to imitate an exact sixth of the rig that is cylindrically repeated, the sides of the 60 degree wedge were set as periodic boundaries. This was done by creating a fluid-fluid interface whose domain spans from one side of the wedge to the other. The interface model was then set to a "Rotational Periodicity" and the rotation axis was selected as the convergence line of the wedge. The remaining default settings of such a fluid-fluid interface were sufficient for this problem.

A default interface was automatically created between the two split bodies of the TCR model geometry, connecting the throttle holes at the locations they were cut. All default settings were sufficient including a conservative interface flux and an automatic mesh connection. However, because the model was cut on a place with three distinct holes, CFX automatically created nine connections for that face. These connections include connections between physically non-connecting holes, such as the top hole on one side and the bottom hole on the other. Thus, under "Connectivity" in the CFX-Pre Outline, these incorrect connections were deleted, leaving only three remaining – top-to-top, middle-to-middle, and bottom-to-bottom. The "Default Fluid Fluid Interface" boundaries also needed to be adjusted to account for the non-overlapping areas of the throttle that exit when the body is rotated. Within each of these boundaries, under the "Nonoverlap Conditions" tab, the "Nonoverlap Conditions" box was checked, and the wall was set as "No Slip Wall," "Smooth," and "Adiabatic." Figure 17 shows the outline setup containing each of the aforementioned items. Figure 18 shows the model with the applied setup within CFX-Pre.

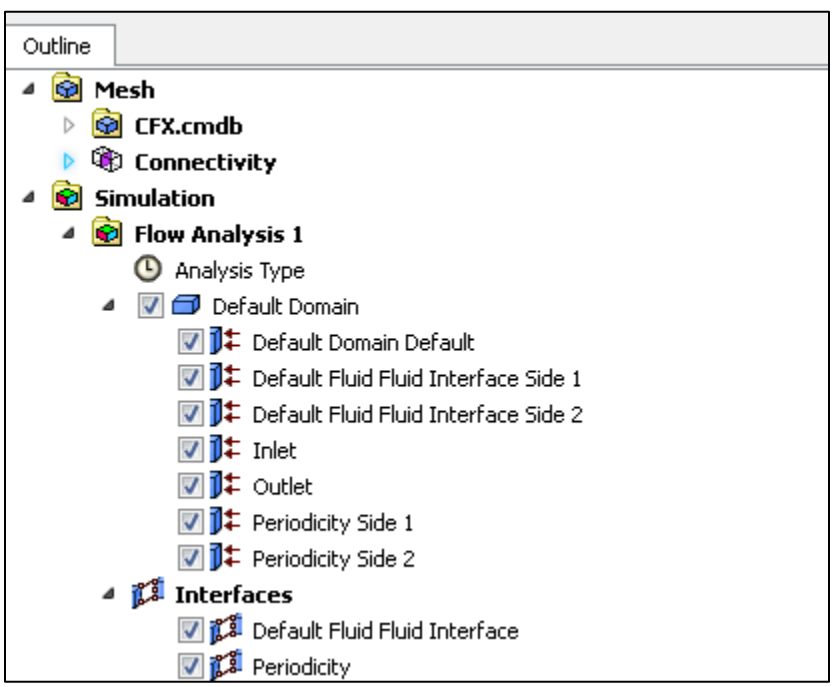

Figure 17. CFX-Pre outline with all defined boundaries and interfaces.

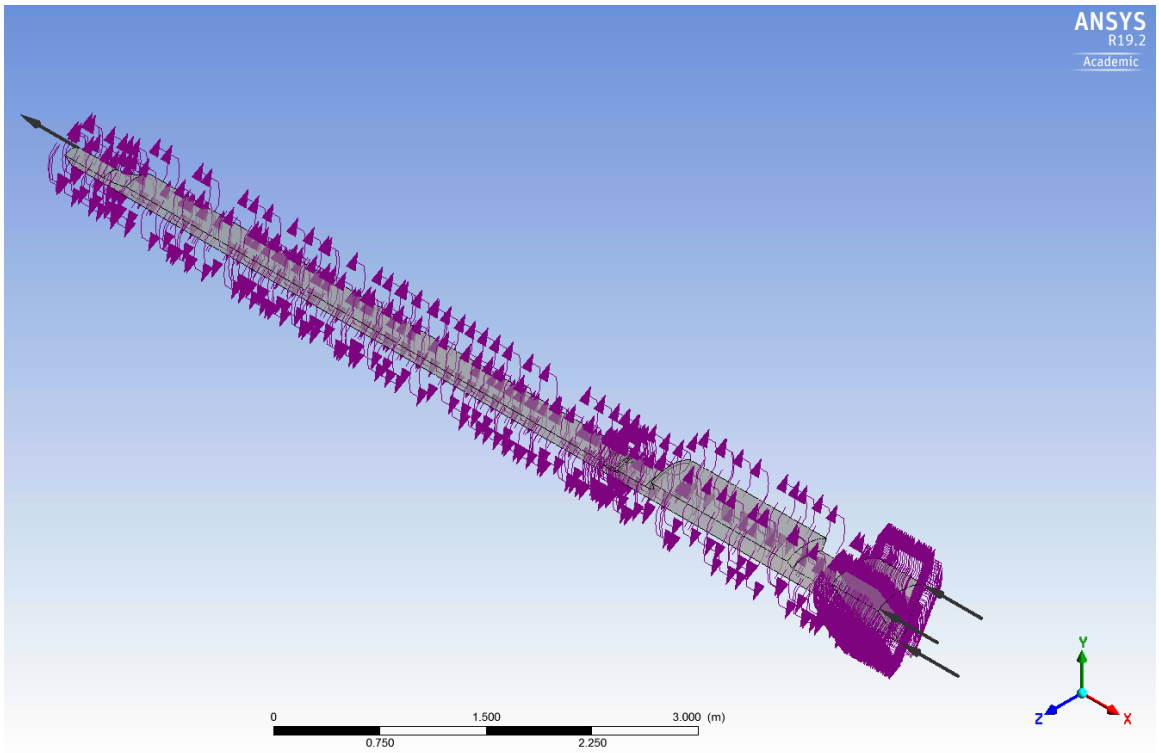

Figure 18. CFX-Pre setup applied to TCR model.

Trial-and-error revealed that the complex mesh and geometry required a smaller timescale factor to avoid a linear overflow error in the CFX solver. Within the "Solver Control," the timescale factor was set to 0.3 within the default "Auto Timescale" control and "Conservative" length scale option sections. In "Advanced Options," the compressibility control was turned on and high speed numerics were used to account for the flow realities of the real TCR in operation.

The length of the TCR model required the activation of an "Expert Parameter" in CFX that accounted for the long distance through which the solver had to iteratively progress. The convergence control and memory control topology estimate factor was increased from its default of 1 to a value of 1.1 to correct this issue. Additionally, for increased accuracy in the solver, the max continuity loops parameter that is used for high speed models was increased to a value of 3.

4. Solution Controls

Each solution's accuracy was analyzed via residual results of the simulations. A monitor was added that recorded the mass flow rate differential between the inlet of the rig and the outlet of the rig over time throughout the simulations. This difference was set as an interrupt control after a set number of required iterations to ensure that the simulation had balanced the flow throughout the model. This interrupt control expression can be seen in Figure 19. The target differential achieved was 1e-03 [kg/s].

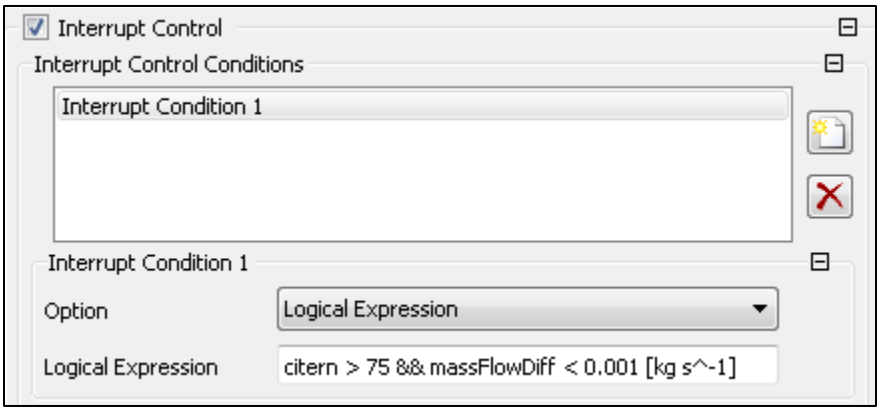

Figure 19. Interrupt control expression used in CFX runs.

Double precision was used in every simulation to increase accuracy and achieve better resolution in the results. Memory allocation factors were increased to values of 1.1. Parallel solving was used to decrease required time in the solutions. Low pressure runs were started using initial conditions for each throttle level setting, however, every high pressure differential used the current solution data available to reduce computational time and increase accuracy.

5. Parameterization

In order to run the simulations for various conditions automatically, two input parameters were designed within the ANSYS Workbench settings. Details concerning how to use parameters in ANSYS Workbench can be found in Thorton [5]. The first parameter was the throttle level. The rotation created on the geometry within the Design Modeler to

mimic the throttle valve locations was selected as an input parameter and could thus be varied for each design point. Additionally, the outlet static pressure used to initiate flow was set as an input parameter in order to vary the total pressure differential across the model. For each rotation, including a zero degree open throttle setting, six pressures were specified. This created a total of 24 design points. To easily tabulate key results of these runs, various output parameters were specified as well through the creation of expressions in CFD-Post.

D. FLOW SCREEN MODELING EXPLORATION

Attempts were made to include in the modeling the layers of porous media that exist within the body of the TCR after the throttle but prior to the mass flow nozzle. The purpose of these screens is to ensure that the flow is parallel through the remainder of the rig and free of any swirling or undesired flow effects. The method used to model these in CFX involved the addition of two porous domains in the geometry—one representing the thinner, denser upstream screen and the other representing the more downstream, hex-shaped screen. The inclusion of these in the geometry and a basic, coarse mesh can be seen in Figures 20 and 21.

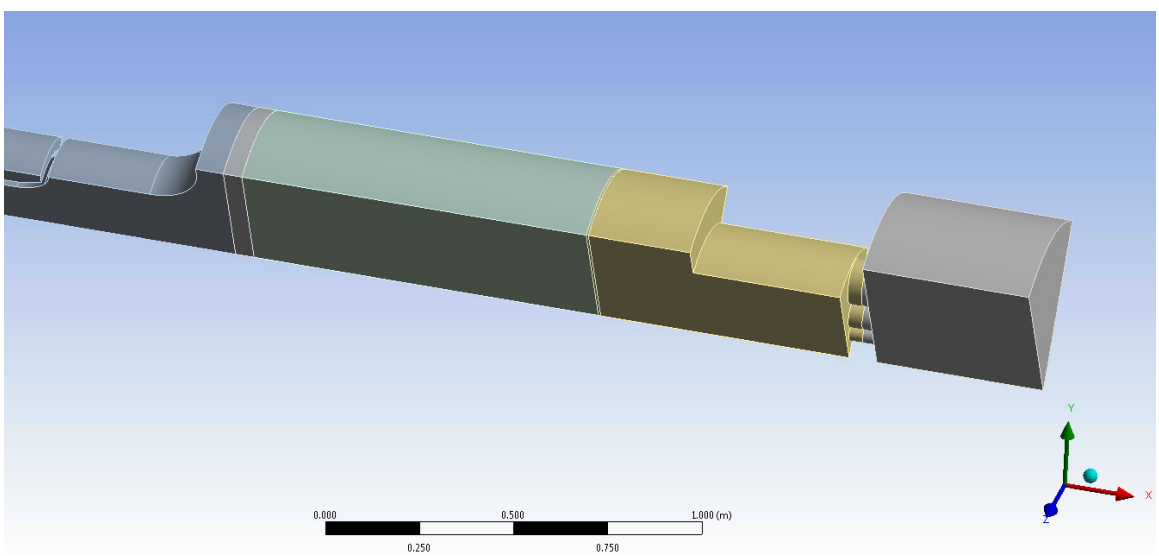

Figure 20. Geometry of TCR model with two flow screens included.

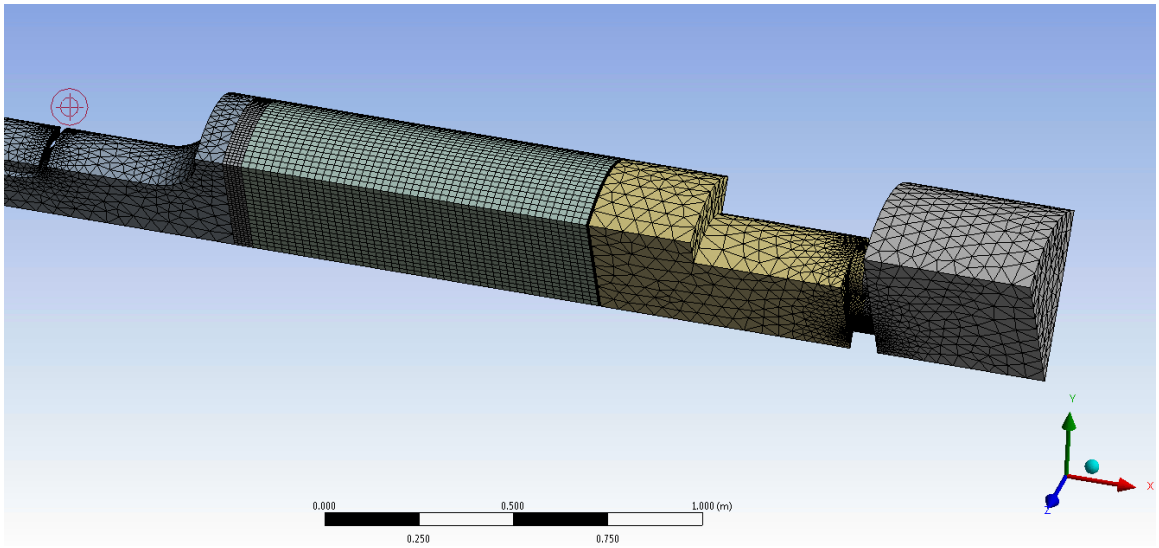

Figure 21. Coarse mesh of TCR model with included flow screens.

The porous domains required inputs for volume porosity, directional losses, and fluid-solid area density. The porosity represents the ratio of fluid volume at the surface of the material to total volume of the material. Setting this value to "1" would equate to a completely open material, while setting it equal to "0" would signify a solid wall of material. The desired loss model was the "Directional Loss" option, signifying in Cartesian coordinates which directions the porous material blocked and which it allowed. In the case of the TCR, these screens ensure the flow through them is solely in the normal direction, and in the case of this model, that direction was in the "x." In CFX setup, the required settings would be [0,1,1] in the directional loss specification. To further define the porous material, an interfacial area density had to be defined as well. This is the surface area of the solid porous material in contact with the fluid over the total solid material volume. For these CFX runs, basic values were given that do not equate to the exact specifications of each flow screen within the TCR. These settings can be seen in Figure 22.

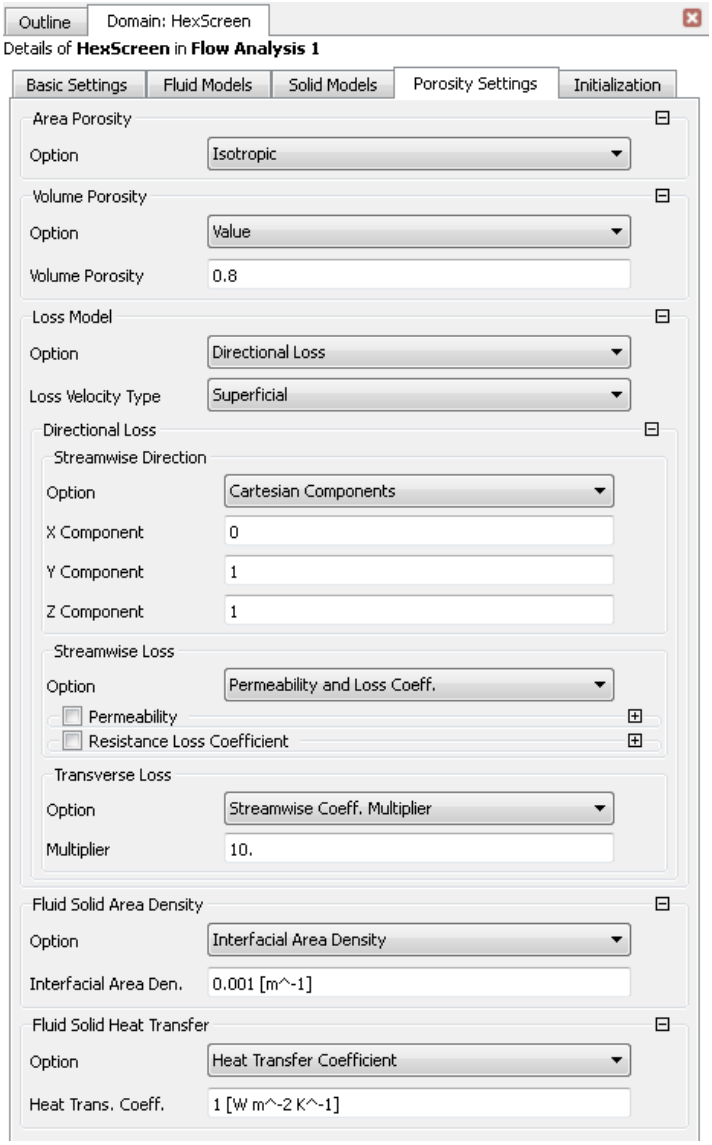

Figure 22. CFX-Pre setup settings for the flow screens included in some model runs.

This model was run with a coarse mesh at low pressure ratios and an open throttle. The flow screen separations created not only the two additional domains of the screens, but also split the remaining domain into smaller sections. The resulting model contained six separate domains, greatly increasing the complexity and increasing the amount of time required for the solver to run. The results seemed promising but did not directly reflect the screens characteristics. Further work is still required in this area.

E. SIMULATION RESULTS

1. High Pressure Issues

At pressure differentials above 10 kPa, the residuals in the CFX solver began to oscillate after 50–100 iterations, slowly rising and no longer converging. Attempts were made to fix the problems by changing the turbulence model, the timescale factor, and various other setup parameters. The issue most likely was formed due to pressure waves beginning to oscillate up and down the long model as CFX attempted to converge onto a solution. The issue was solved by prescribing a mass flow rate at the inlet as opposed to the total pressure specified for the lower pressure differentials. In order to find the correct mass flow rate for the given pressure, the standard setup was used for lower pressure differentials under 15 kPa to acquire mass flow rates to form the quadratic performance curve. The mass flow rates for higher pressures, then, found from this curve, were used to initiate the model. This allows the flow to be fully analyzed for other characteristics at these higher pressure differentials. The method was effective for all throttle angles with a coarse mesh size. However, issues arose when the finer mesh was used, as the solver was unable to run due to a "fatal linear overflow error" in the CFX solver. Further work would need to be done to investigate the issues that caused this error. Thus the data presented in the pressure cases above 10 kPa is data run on a coarser mesh than the rest of the CFX simulations.

2. Mass Flow Rates and Mach Numbers

The mass flow rates found were used to plot the performance curves for each throttle setting tested. These curves can be seen in Figure 23. The tabulated data can be seen in Appendix G along with other important output parameters.

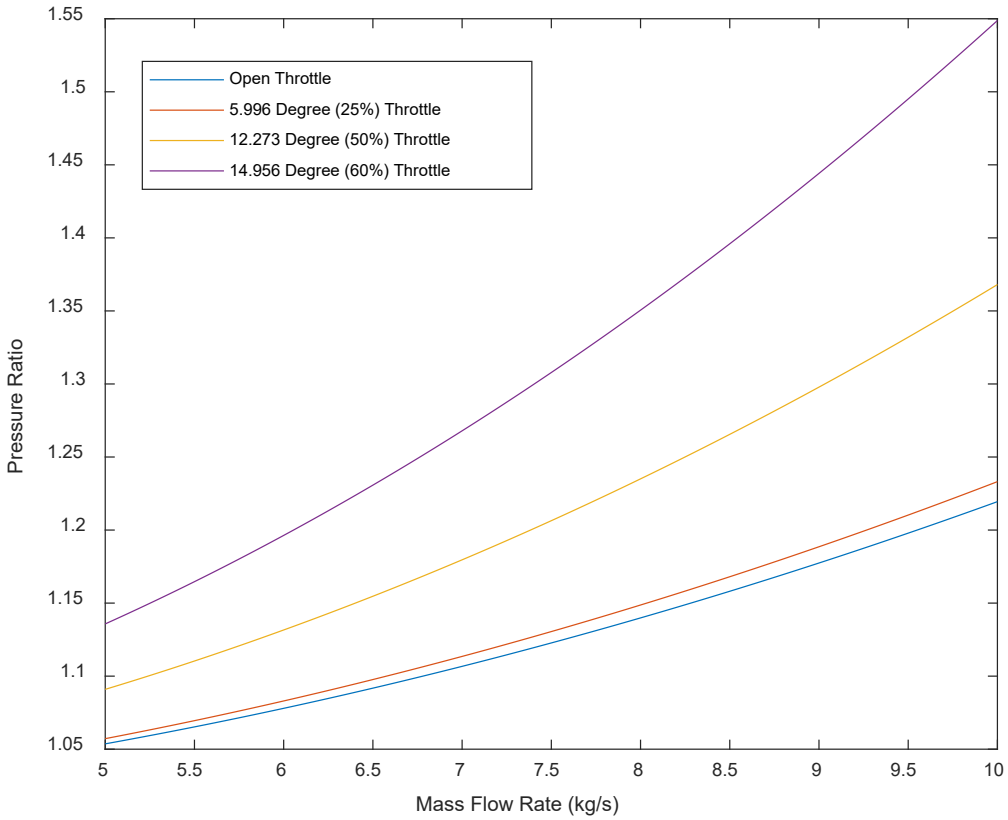

Figure 23. Mass flow rate curves derived from CFD flow analysis

These curves show the expected quadratic shape and were derived from low pressure ratio runs of the CFD model. The plot in Figure 23 shows the range of mass flow rates found experimentally at the various compressor speeds tested.

The maximum Mach numbers for each throttle setting and pressure differential can be seen in Appendix G. As expected, the maximum Mach number increased as the throttle area decreased, and within each throttle setting it increased with increasing pressure ratios. The highest Mach numbers were found around the throttle point where the flow was forced through the limited-area openings as well as the final bell mouth leading into the compressor face. Figures 24 and 25 show the Mach number profiles throughout the TCR model for a 10 kPa pressure differential for an open throttle and a 25 kPa pressure differential for a 12.273 degree rotated throttle, or 50% covered.

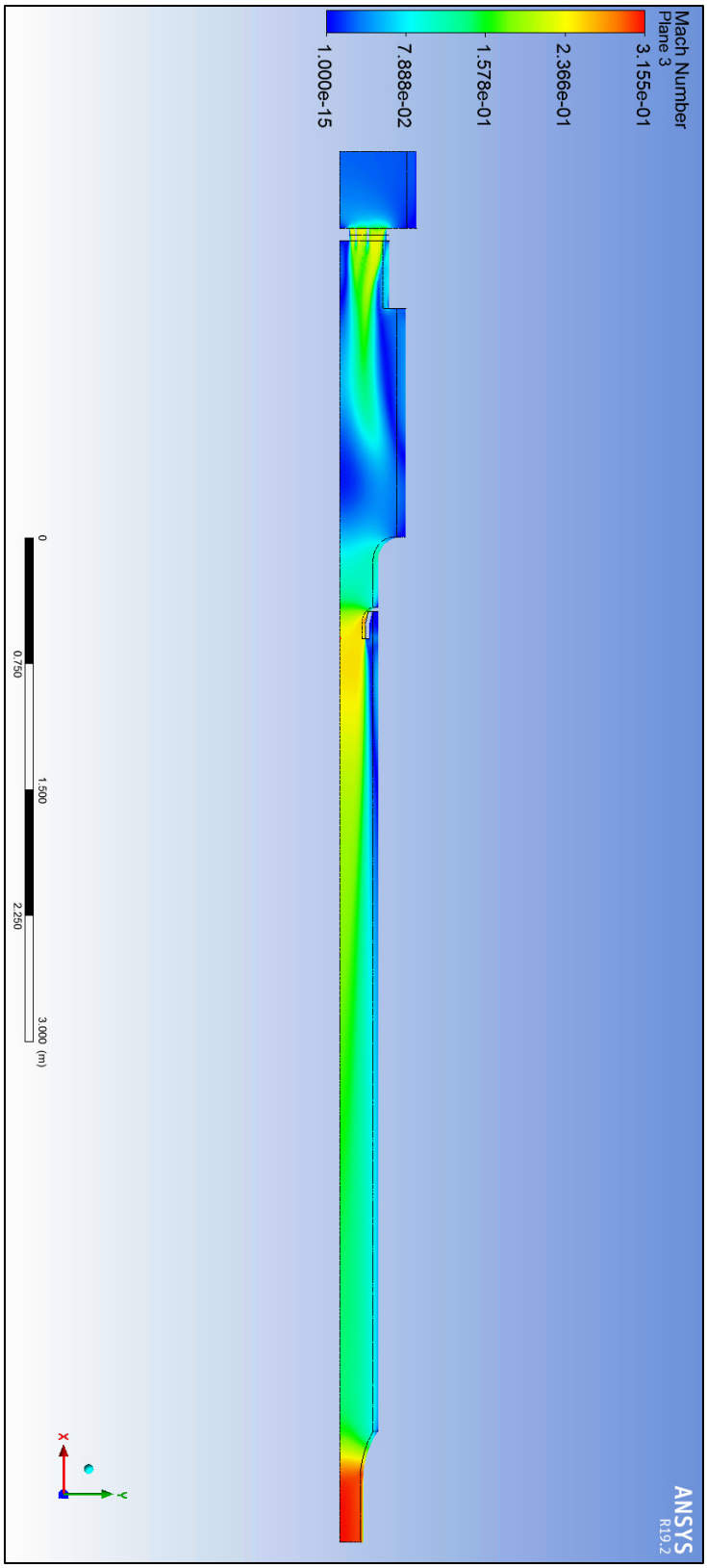

Figure 24. Mach number profile for 10 kPa and an open throttle.

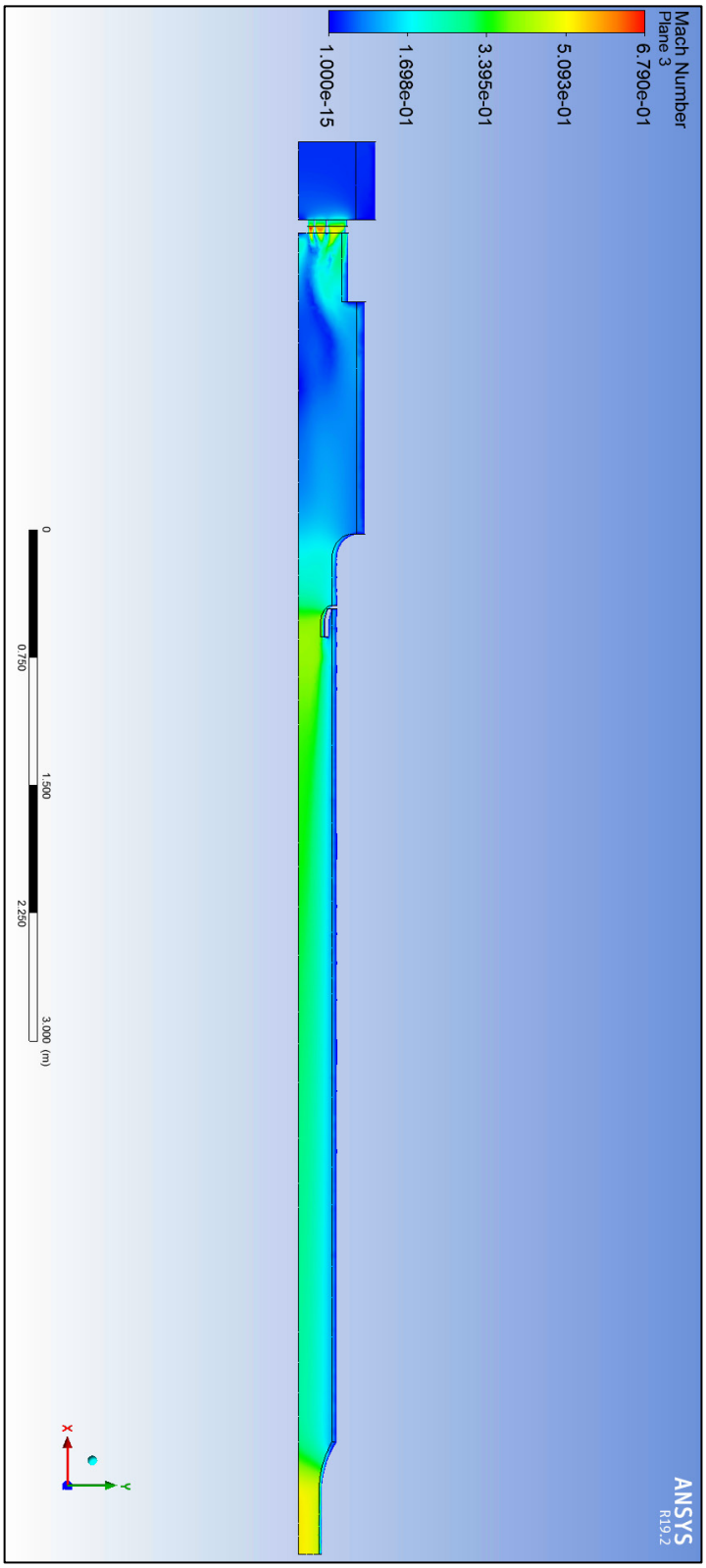

Figure 25. Mach number profile for 25 kPa and 12.273 degree rotated throttle (50% covered).

The flow can be seen accelerating through the throttle and reconnecting in the main body of the TCR before accelerating through the mass flow nozzle further and again through the bell mouth into the compressor face. The flow shows some swirling after its acceleration through the throttle in both cases, although the disruption in the flow becomes much more apparent in the higher pressure differential case and tighter throttle case. As the pressure differential increased and as the throttle tightened, the flow's movement increased. This is important to note as this model is being run without the implemented flow screens meant to limit any flow swirling within the rig.

3. Pressure Profiles at Measurement Locations

Pressure probes are used around the nozzle in the middle of the TCR to measure the stagnation pressure at the wall immediately before the nozzle and the static pressure about 0.0254 meters (1 inch) behind the static pressure. These pressures were also measured in the CFD model results, and their locations can be seen highlighted in Figure 26.

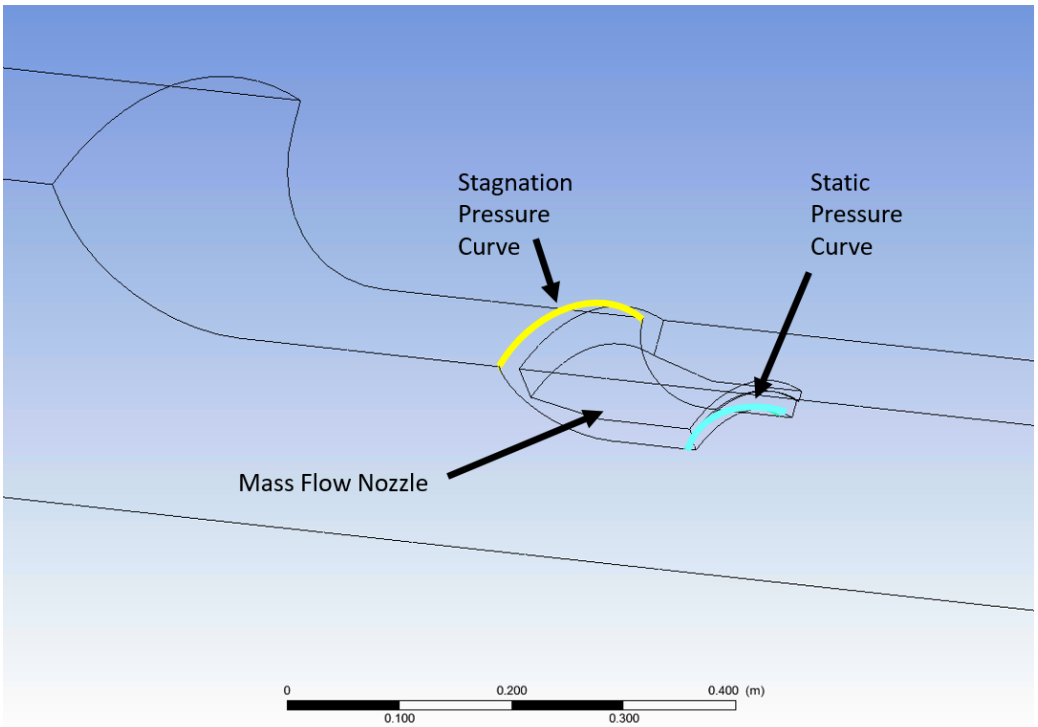

Figure 26. Stagnation and static pressure curve locations.

The probes assume that the pressure at those measuring planes is axisymmetric, making their location around the wall of the TCR irrelevant. It was important, however, to check this assumption by observing the pressure profiles of the simulated CFD runs. The stagnation and static pressure profiles for the 10 kPa, open throttle run are shown in Figures 27 and 28.

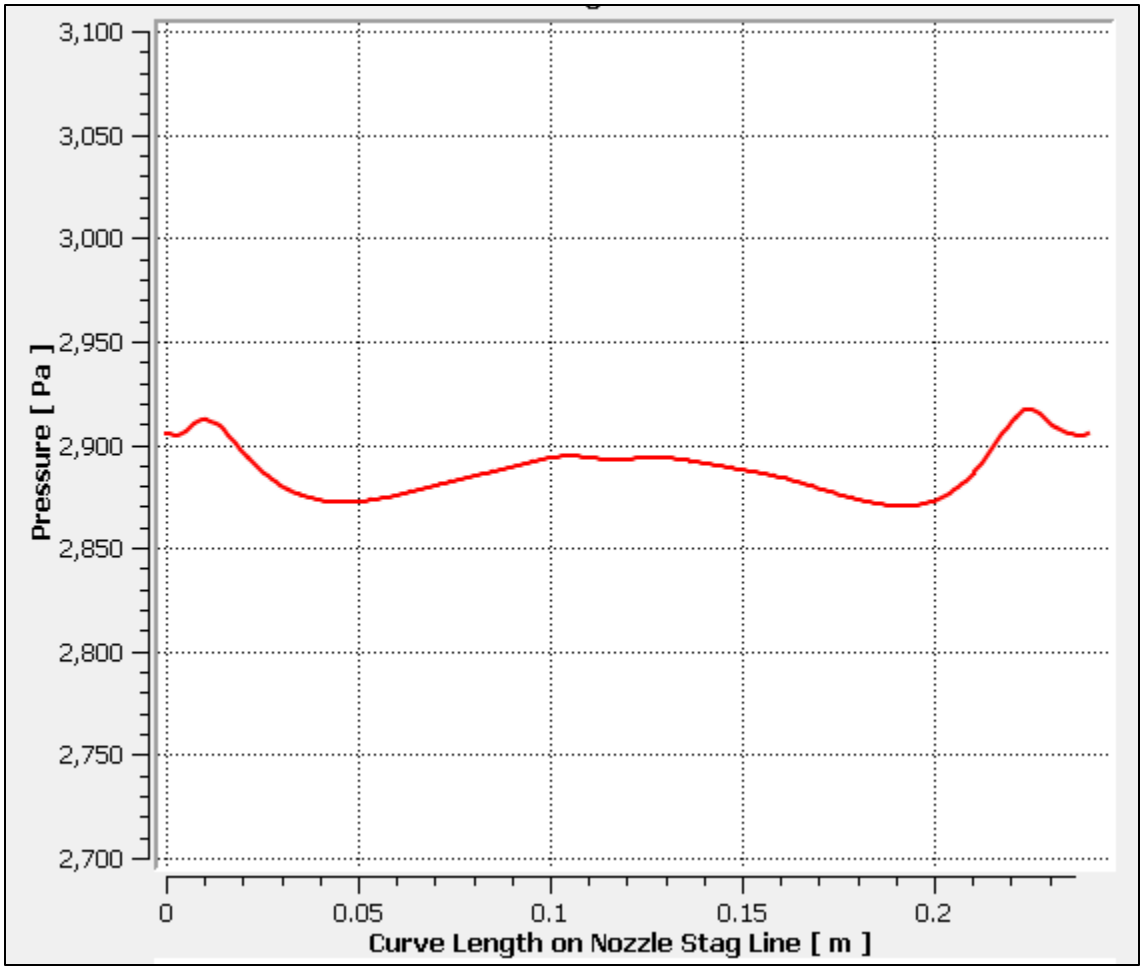

Figure 27. Stagnation pressure profile over the length of the stagnation pressure curve from CFD simulation.

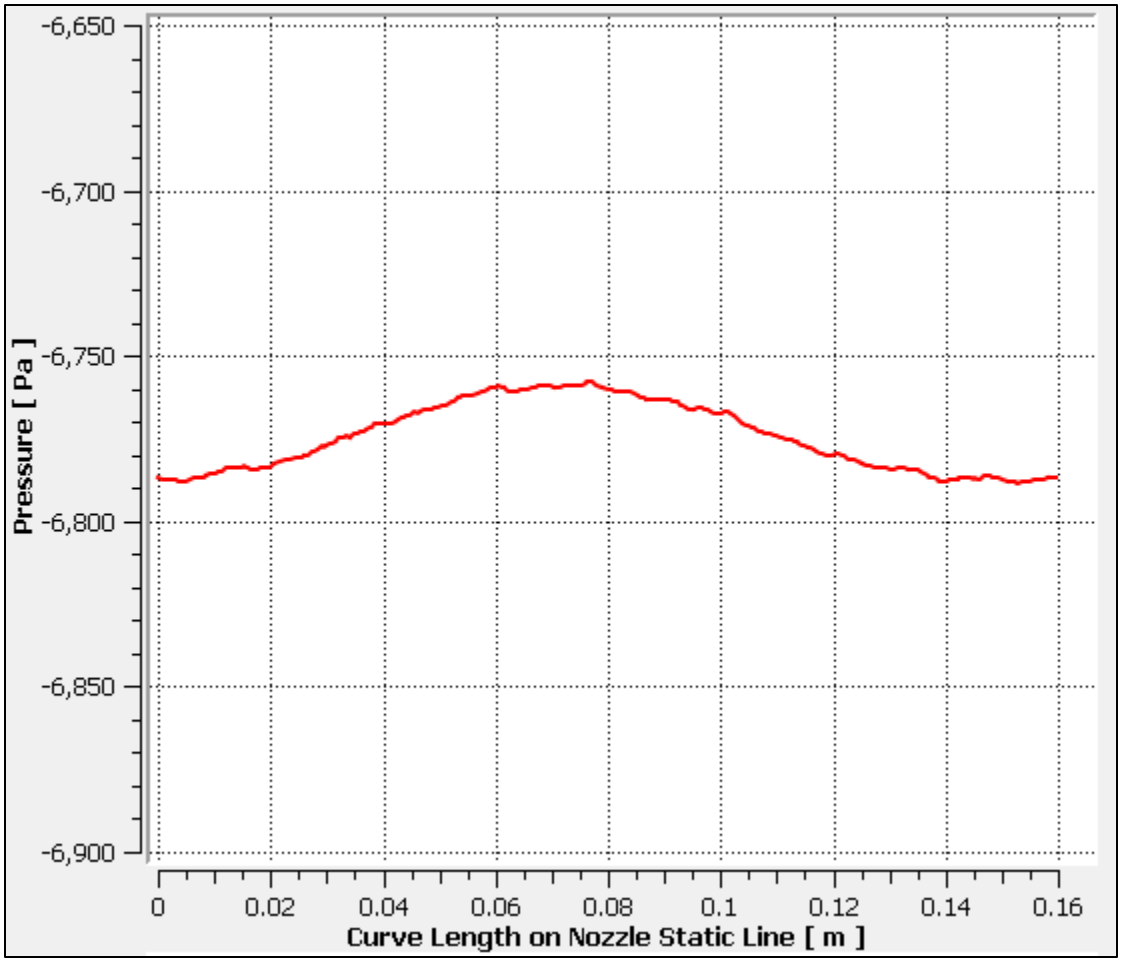

Figure 28. Static pressure profile over the length of the static pressure curve from CFD simulation.

These profiles show that the flow is in fact axisymmetric in its pressure at these locations. The spread of values in each of these plots is very low, with a maximum difference of less than 50 Pa, or less than 1% of the specified outlet pressure. The minor differences over these profiles with respect to the uncertainty of the measurement probes confirm that their location around the wall have a negligible effect on the measurement of the mass flow rate at the nozzle.

4. Turbulent Kinetic Energy Profiles

Another aspect of the flow investigated through the CFD simulations was the turbulent kinetic energy at the exit plane of the mass flow nozzle. If the flow was properly

paralleled at this point and not disturbed in any unexpected ways, the profile of the turbulent kinetic energy would show a smooth gradient from the wedge tip up to the wall. It would then show a spike followed by a steep drop to zero as the flow reached the laminar sublayer and the non-slip wall. Figures 29 and 30 shows the nozzle exit plane and the turbulence profile for the 10 kPa, open throttle case.

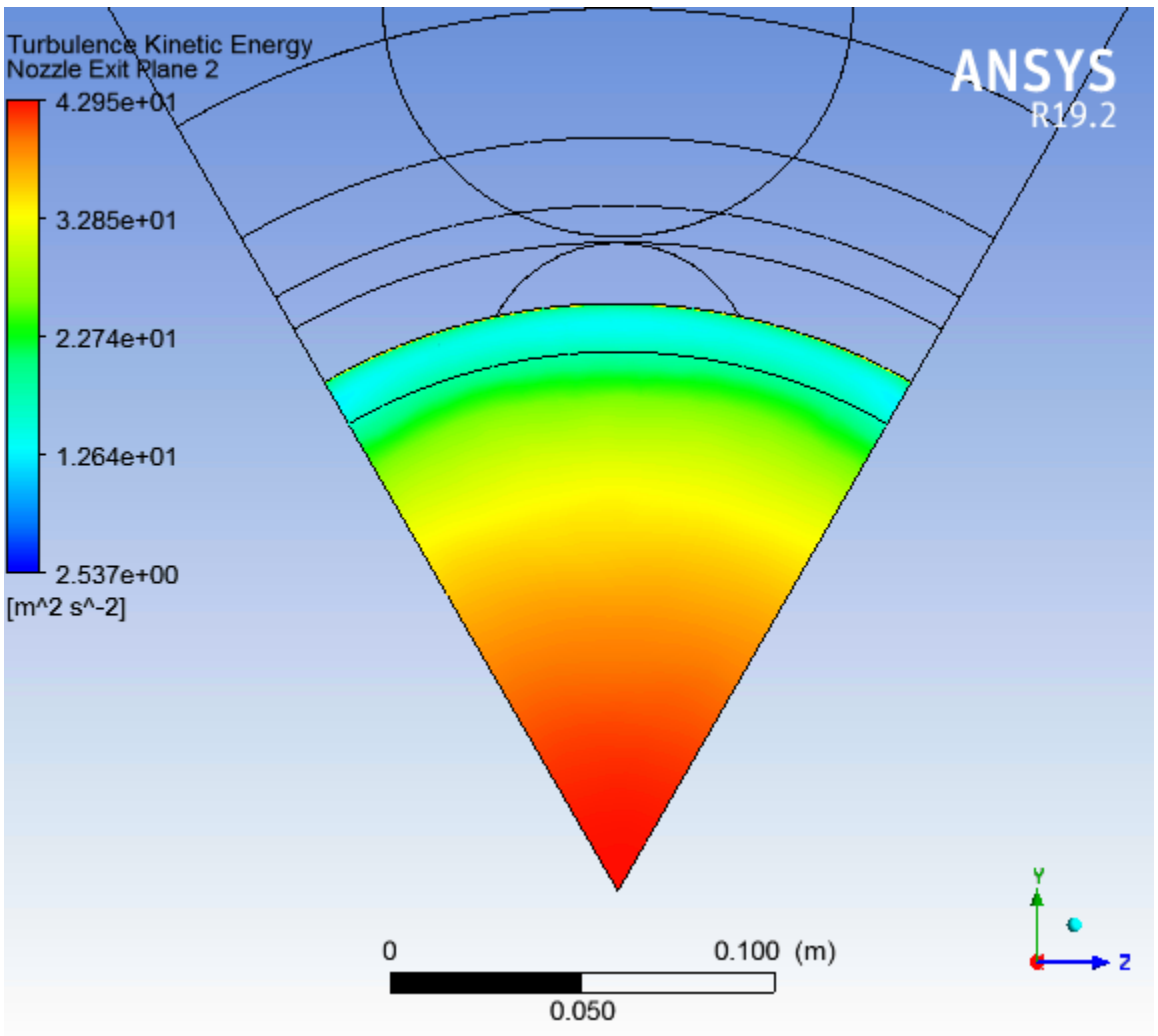

Figure 29. Turbulent kinetic energy color map at the nozzle exit plane.

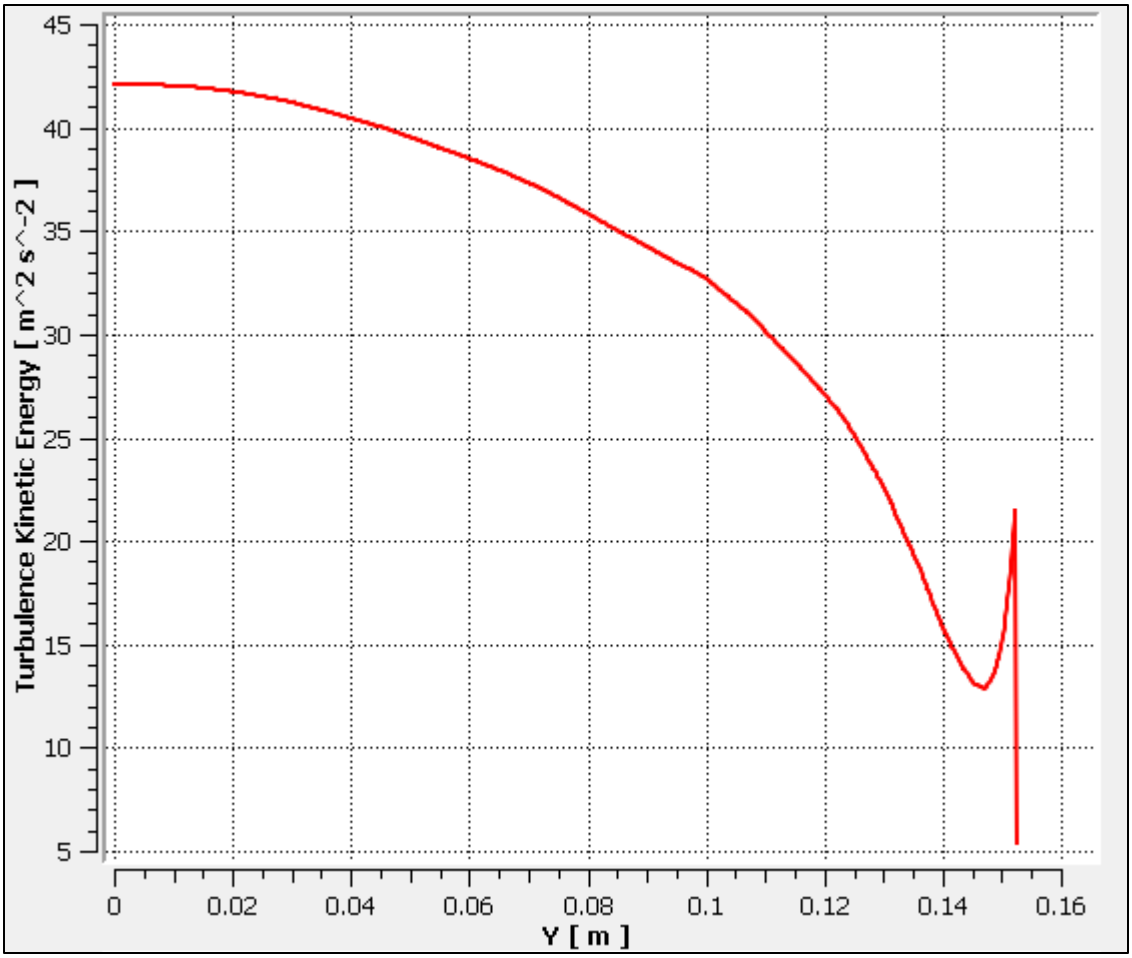

Figure 30. Turbulent kinetic energy profile over the vertical distance from the wedge tip to the wall of the model.

These profiles demonstrate the expected performance of the flow at the nozzle exit plane, confirming that no undesired turbulence is affecting the mass flow rate measurements at the nozzle.

Additional data on each of the runs can be found in Appendix G.

V. EXPERIMENTAL RESULTS

A. DATA RUNS SETUP

The NPSMF was run through the TCR for four different speeds: 70%, 80%, 85%, and 90% of the compressor's maximum speed. The runs were conducted using a smooth casing causing no flow disturbance into the compressor face. The method of testing involves creating a pressure difference from the atmospheric inlet pressure of the TCR through the operation of the rotor at an open throttle. This process is done isothermally, as no work is put into the flow until it reaches the compressor. At this point, the compressor heats up the flow and returns it to a pressure above atmospheric pressure, dumping the excess kinetic energy. This process can be seen in the T-s diagram shown in Figure 31.

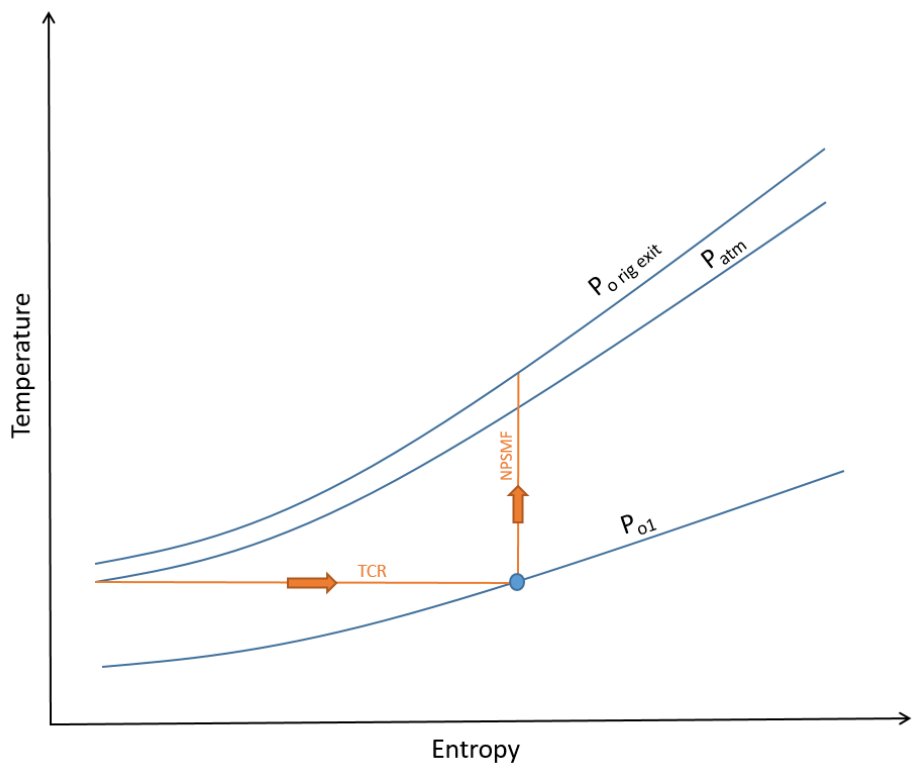

Figure 31. T-s diagram for TCR and NPSMF operation.

Through the testing, the throttle is set to more closed settings and steady-state data is acquired at each throttle level until the compressor reaches stall due to the decrease in mass flow rate. The raw data from these runs is recorded and subsequently fed through post-processing MATLAB scripts to identify measurement errors, malfunctioning probes, or oddities in the data. These scripts also analyze and plot the desired characteristics.

B. PERFORMANCE CURVES AND EFFICIENCIES FOR NPSMF

One of the most important characteristics that the TCR is used to demonstrate is the performance of the compressor being tested. By measuring the pressures around the nozzle and the pressures at the NPSMF inlet, the mass flow rate into the NPSMF was recorded. This was then scaled to account for any differences in conditions within the TCR from standard atmospheric operating conditions. The pressure ratio between the NPSMF rotor face and the inlet is recorded and scaled appropriately along with the mass flow rates, both according to the relationships described in Thorton [5]. Figure 32 shows the scaled performance curve for the 70% speed run of the NPSMF. The performance curve for the remaining 3 test speeds can be found in Appendix H.

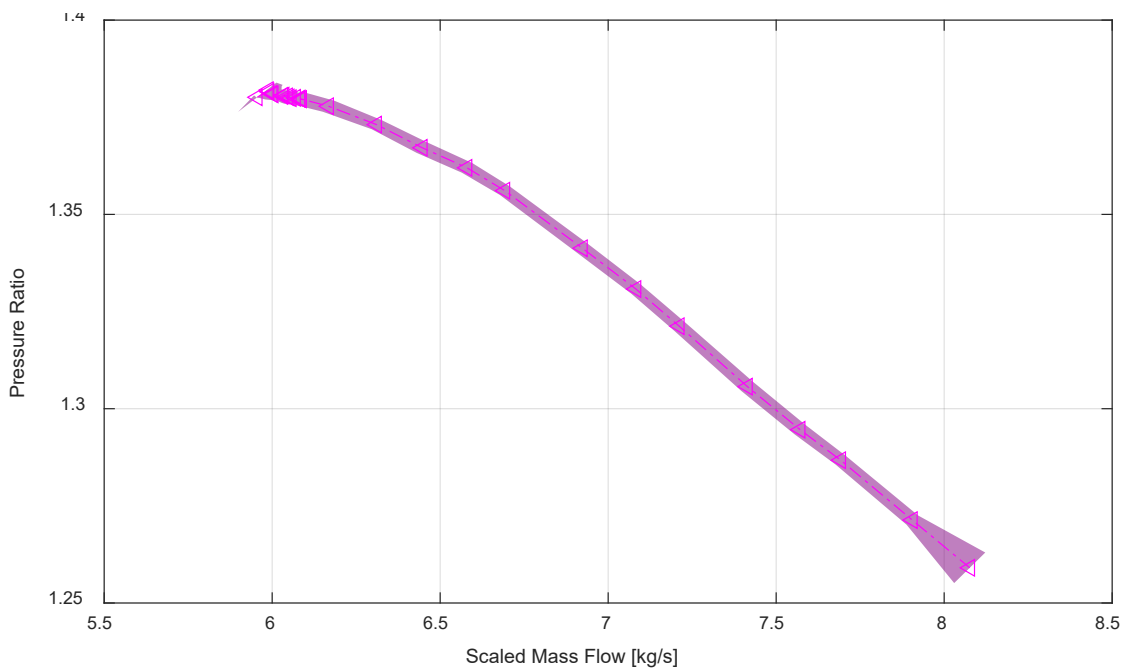

Figure 32. Performance curve of NPSMF at 70% speed +/- 1σ.

Additionally, these performance curves could be used to compare to the mass flow rate curves acquired through the CFD simulations. The unscaled values of pressure ratios and mass flow rates were used. The pressure ratio was calculated as the recorded inlet pressure over the averaged static pressure at the compressor's face, taken from the raw data file as "Ps1_avg." The mass flow rate used is identified in the raw data file as "m_dot_X." The overlaid curves can be seen in Figure 33.

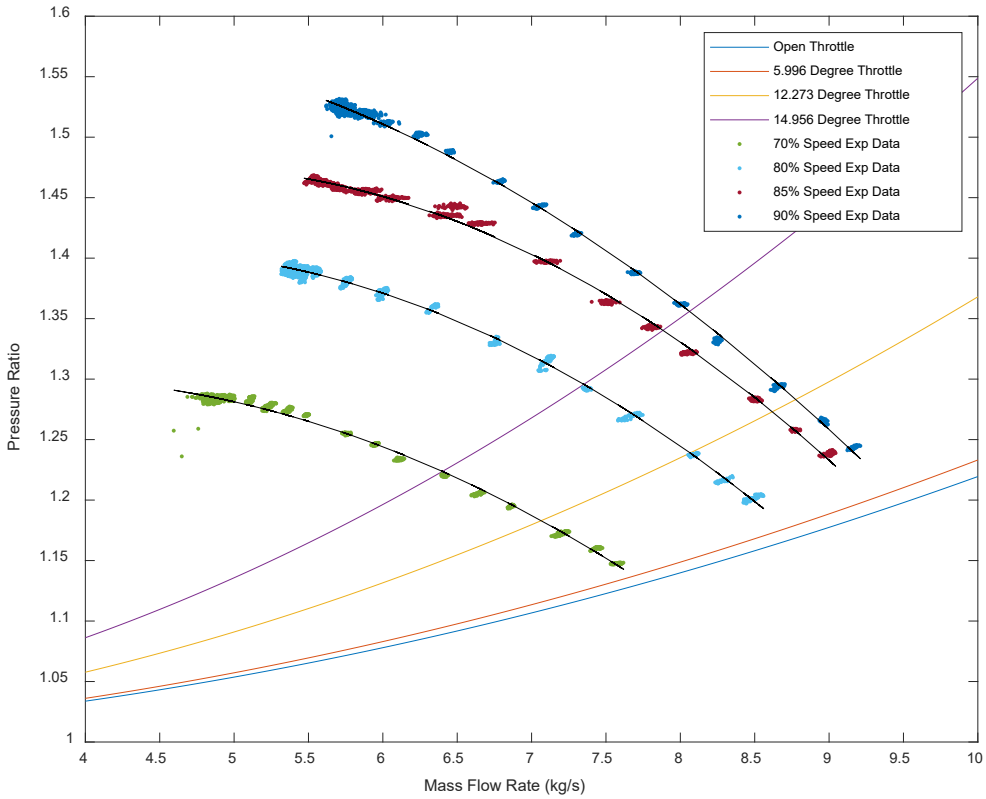

Figure 33. Overlay of performance curves from experimental data and mass flow rate curves from CFD analysis.

The figure above shows that the CFD model produces fewer losses in pressure drop than the actual performance curve of the NPSMF. This was expected, as the flow screens were not included in these results, and their presence would cause a further pressure drop in the TCR. The figure does show that the CFD model produced respectable mass flow predictions, however, when compared to the experimental data, as the curves do intersect

in the testing pressure ratio spectrum and mass flow rate values recorded. Further work can add the additional components of the TCR that would provide the losses not accounted for here.

Another important characteristic that was calculated and recorded for the NPSMF was the mass averaged efficiency. The mass averaged efficiency curve for the 70% data run can be seen below in Figure 34. In the calculation of the efficiency curves for the NPSMF, the thermocouples indexed in the raw data as “T 8” and “T 10” were removed from the calculations due to bias errors in their measurements. The remaining curves for the other speeds can be seen in Appendix I.

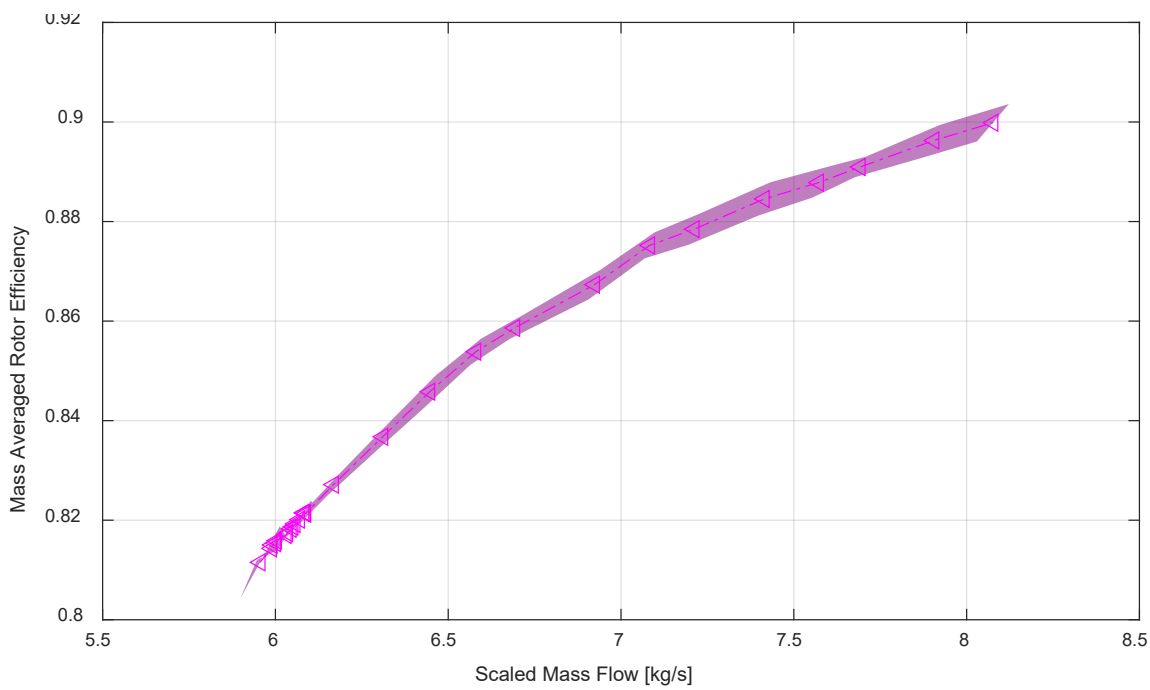

Figure 34. Mass averaged efficiency of NPSMF at 70% +/- 1σ.

VI. CONCLUSION

A. SUMMARY

The goal of this thesis was to increase confidence in the mass flow rate measurements of the TCR while providing a robust computational model for future use to explore other aspects of the rig. The design of the bell mouth attachment will allow this goal to be pursued further upon its implementation. The CFD results of the TCR model confirmed assumptions regarding the flow dynamics through the mass flow nozzle and provided significant upstream data for future testing. The pressure profiles around the nozzle further affirmed the placement of the probes for measuring mass flow rate. The performance curves affirmed the validity of the CFD model while revealing its need for additional components to account for other losses in the flow.

B. RECOMMENDATIONS FOR FUTURE WORK

Further investigation ought to be pursued into the causes for overflow errors in high pressure ratios within the CFX model. Significant work was put in to trying to rectify the problems, however no solution was found. The lower pressures converge well, while each higher pressure failed to do so, oscillating up to larger residuals.

The implementation of the flow screens in the CFD model would continue to increase the analysis' accuracy and provide more comparable flow to experimental data and pressures. The basics of the model have already been implemented, but these screens must have the proper porosity and interfacial area density calculated and then specified within CFX. Computational time will be large for this kind of model.

Upon the implementation of the bell mouth attachment, this attachment ought to replace the inlet in the CFX geometry. The data around that inlet bell mouth can then be compared to experimental data recorded once it is in operation, and the CFD model can then be checked to ensure accuracy.

THIS PAGE INTENTIONALLY LEFT BLANK

APPENDIX A. ASME MFC-26-2011 BELL MOUTH INLET FLOWMETERS GUIDELINES

This Standard is centered around the typical method of flow calculation in a bell mouth via pressure and temperature measurement at the bell mouth's throat. The Standard defines the throat of the bell mouth as "the axial portion of the bell mouth of constant diameter" [7]. At the throat, the Standard specifies that the free-stream conditions ought to be directly measured axially and measured radially such that the points are not in the boundary layer. All sensing points of the inserted probes ought to be positioned within the same axial plane "at a distance greater than 0.5*d* downstream of where the flared inlet ends,…although 1*d* or greater is recommended" [7]. These probes ought to be positioned so as to not interfere with or disturb the wall static taps as well.

In terms of quantity, larger bell mouths require more probes. However, four equally circumferentially spaced probes is sufficient, while two may be adequate for small diameter bell mouths. The same guidance is applied to static pressure taps. For the purposes of this research, the bell mouth attachment was designed for four static pressure taps only. It was designed to follow the "Clean Inlet Method" referenced in this Standard. This method assumes low air velocity and infers the total pressure and temperature at the throat from ambient conditions.

Fluid properties that can affect the flow rate measurement are specified including density, viscosity, isentropic exponent, and thermal expansion. The effect of the size of the bell mouth on the flow conditioning is also explained. The Standard recommends additional flow conditioning downstream of the bell mouth for any throat diameters less than 0.508 meters (20 inches).

The bell mouth ought to be made out of corrosion-resistant material. For high-temperature uses, stainless steel is recommended. For normal operations, aluminum or composite materials such as fiberglass may be used.

For the machining of the bell mouth, special care should be given to the bell mouth throat. It ought to be as cylindrical as possible, with any taper not exceeding -5.08e-5

meters (-0.0020 inches) for diameters larger than 0.1524 meters (6.00 inches). Tapers must err on the negative side, decreasing the throat diameter towards the outlet. In terms of surface roughness, in order to ensure fully developed flow with low wall friction, the surface finish, R_d, below should be followed.

$$R_d = 10^{-5} * d$$

where d = bell mouth diameter

APPENDIX B. BLAIR AND CAHOON BELL MOUTH DESIGN

This study focused on the best practices to optimize the design of an intake bell mouth by using CFD software and comparing various shapes and inlet conditions. The characteristics used to evaluate these bell mouths were mainly C_D and mass flow rates.

The three most common bell mouth configurations were analyzed and can be seen in Figure 35. These are the simple circular radius, the gradually expanding aerofoil, and the elliptical-shaped profile.

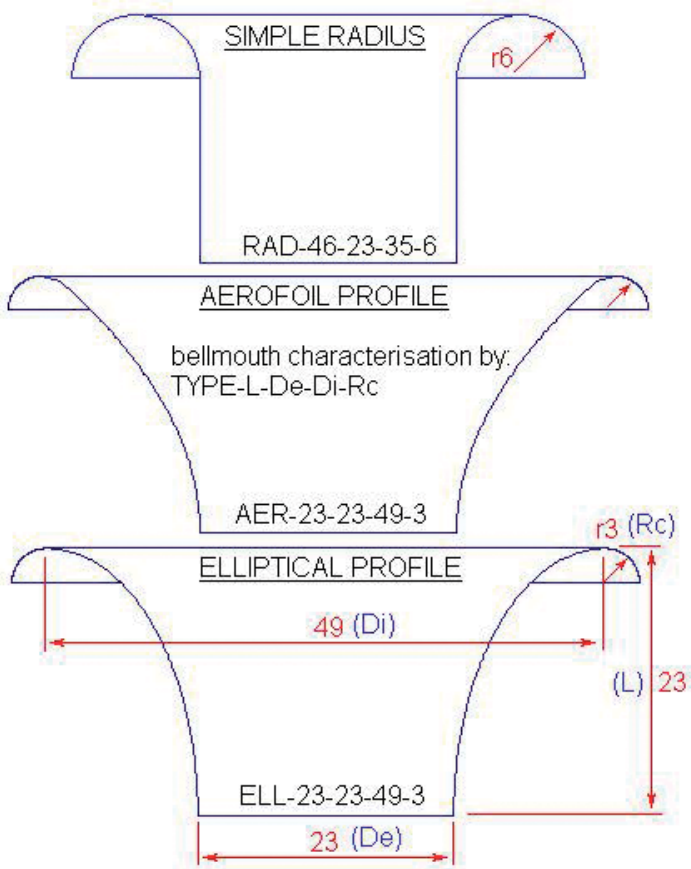

Figure 35. Three bell mouth shapes tested by Blair and Cahoon [8].

A wide range of dimensions for these three configurations were tested at various pressure ratios. In order to most easily observe the results, the C_D values and mass flow

rates with a set pressure ratio were plotted as a percentage of improvement from the most simple radius bell mouth, identified as RAD-46-23-35-6 in Figure 35. These results can be seen in Figures 36 and 37.

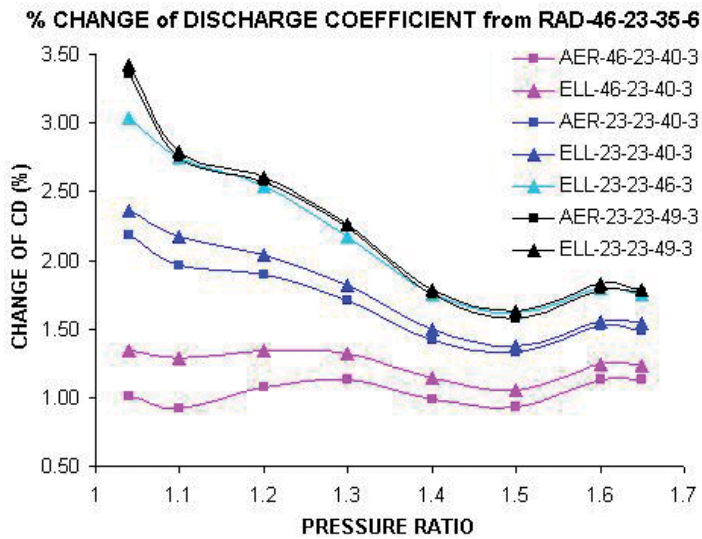

Figure 36. C_D improvements for each bell mouth shape tested by Blair and Cahoon [8].

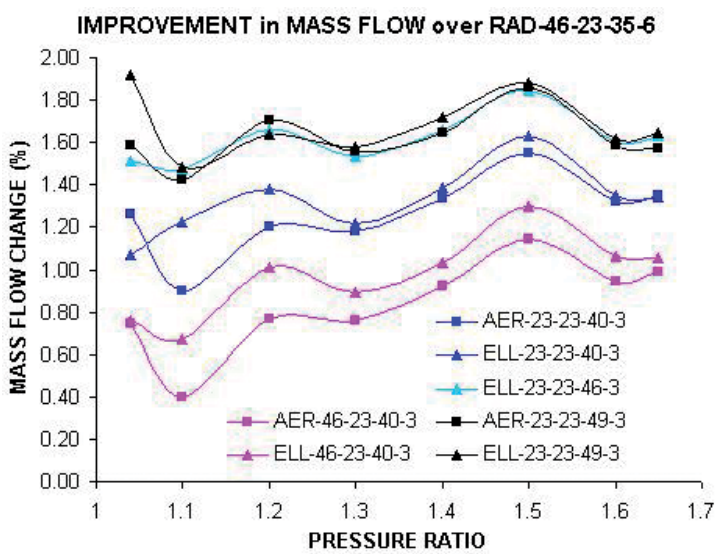

Figure 37. Mass flow rate improvements for each bell mouth shape tested by Blair and Cahoon [8].

The ultimate conclusion is that the “short and fat” elliptical bell mouth, identified as ELL-23-23-49-3 in the plots above, had the greatest percentage improvement over the simple radius bell mouth. This shaped bell mouth is thus the “best” bell mouth as defined by the C_D and mass flow rates standards presented by Blair and Cahoon [8]. They note, however, that the advantage is slim, with an improvement percentage of a mere 2.5% in C_D and 1.5% in mass flow rate.

This “short and fat” elliptical shape of approximate 2-to-1 ratio between entry and exit diameters was used for the design expanded upon in this thesis.

THIS PAGE INTENTIONALLY LEFT BLANK

APPENDIX C. CYLINDRICAL CASING DRAWINGS

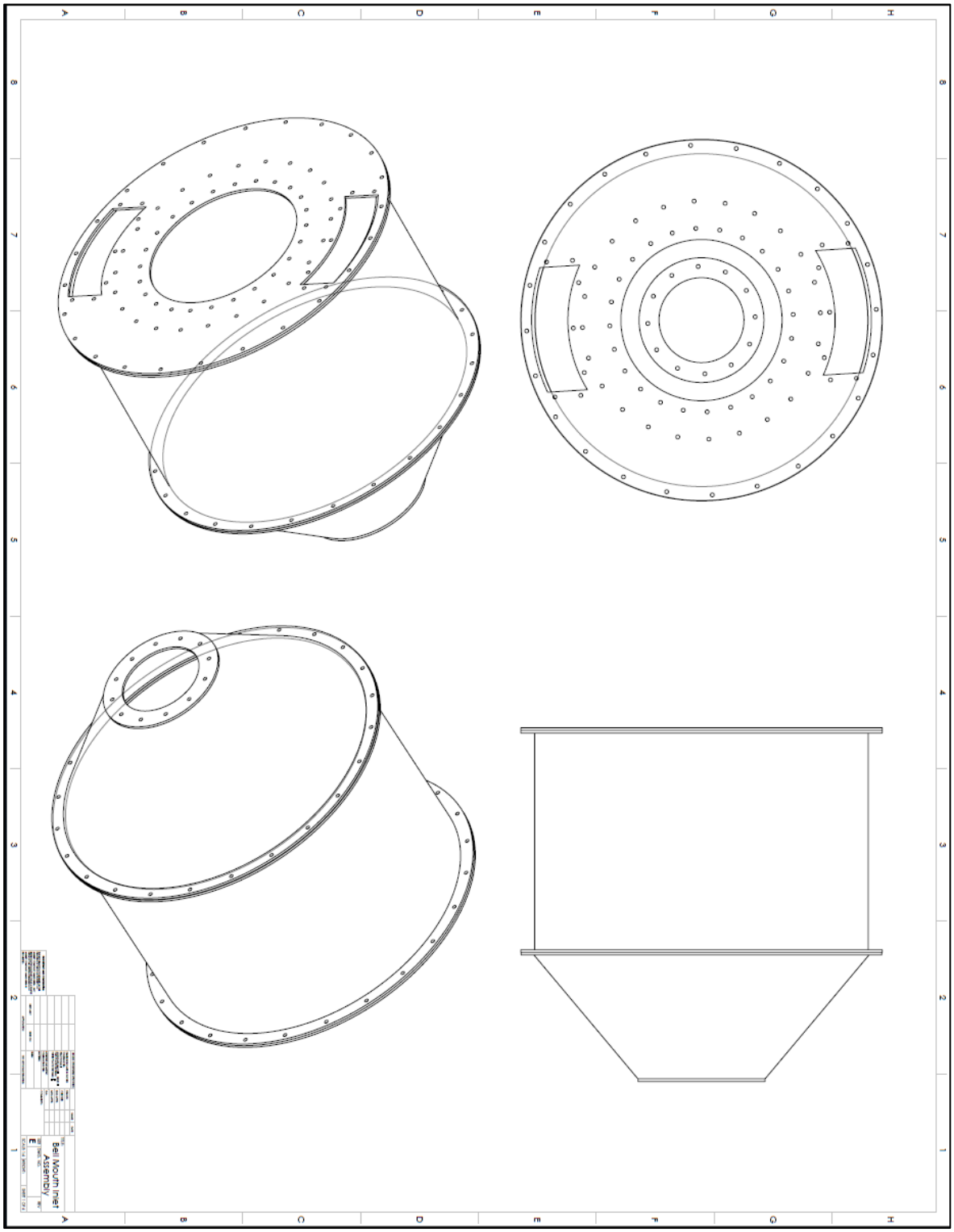

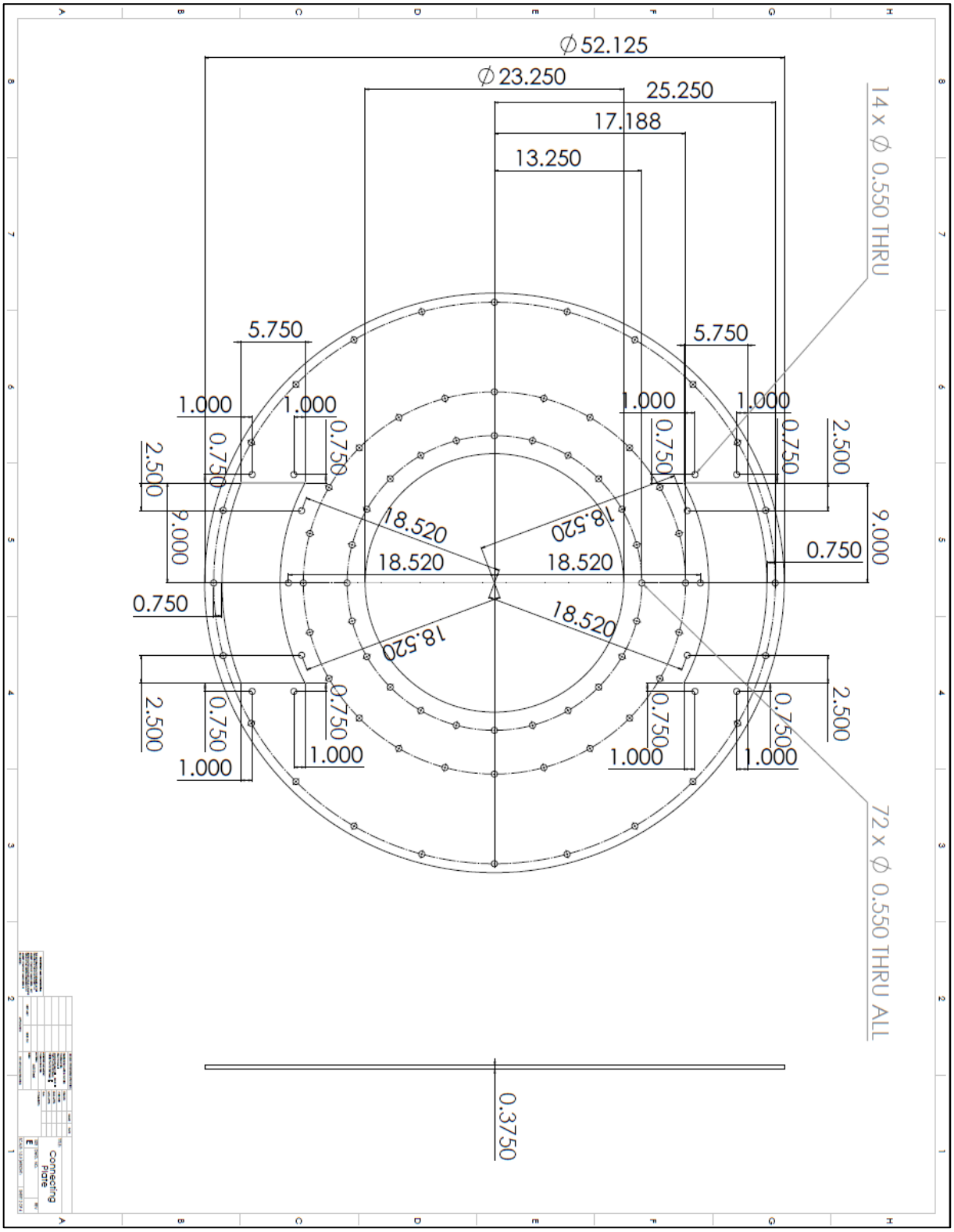
∅52.125
∅23.250
25.250
17.188
13.250
14 x ∅ 0.550 THRU
5.750
5.750
1.000
1.000
1.000
1.000
0.750
0.750
0.750
0.750
2.500
2.500
9.000
9.000
18.520
18.520
18.520
18.520
0.750
0.750
2.500
2.500
0.750
0.750
0.750
0.750
1.000
1.000
1.000
1.000
72 x ∅ 0.550 THRU ALL
0.3750
Connecting Plate
E

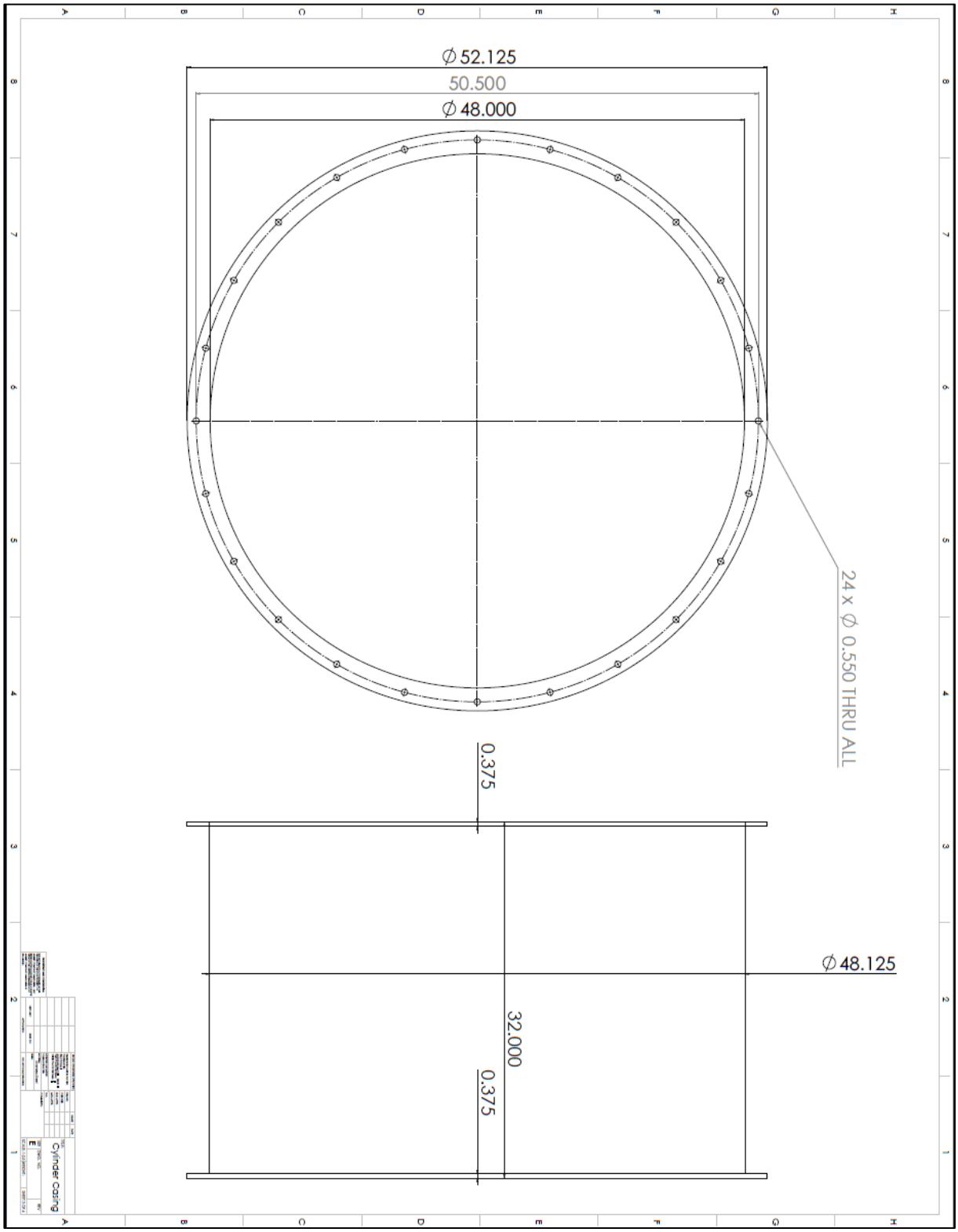
Cylinder Casing
E
Ø 52.125
50.500
Ø 48.000
24 x Ø 0.550 THRU ALL
0.375
Ø 48.125
32.000
0.375

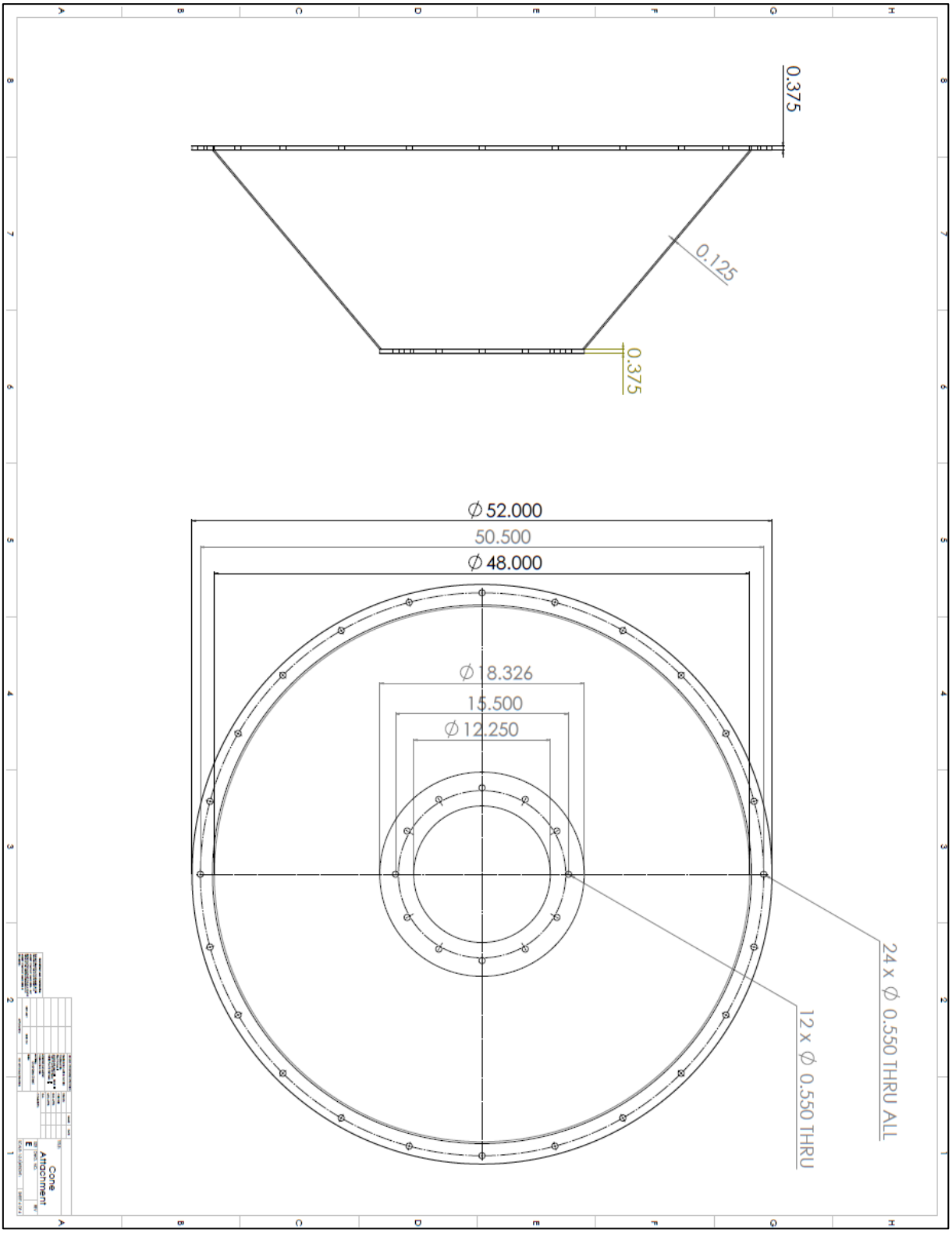
0.375
0.125
0.375
∅ 52.000
50.500
∅ 48.000
∅ 18.326
15.500
∅ 12.250
24 x ∅ 0.550 THRU ALL
12 x ∅ 0.550 THRU
Cone
Attachment
E

APPENDIX D. BELL MOUTH COMPRESSIBLE FLOW CALCULATION

The bell mouth exit sizing was determined by calculating the diameters required to form a given pressure ratio and mass flow rate via compressible flow equations. Using the non-dimensionalized velocity "X" shown below, the density and velocity of compressible flow can be found. These relationships can be seen below also.

$$X = \frac{v}{v_o} = \sqrt{1 - \left(\frac{P_1}{P_{t1}}\right)^{\frac{\gamma-1}{\gamma}}}$$

$$v = v_o X = \sqrt{2c_p T_o}\sqrt{1 - \left(\frac{P_1}{P_{t1}}\right)^{\frac{\gamma-1}{\gamma}}}$$

$$\rho = \frac{P_o}{RT_o}\left(\frac{P_1}{P_{t1}}\right)^{\frac{1}{\gamma}}$$

Using these relationships and the definition of mass flow rate, the area required was calculated according to the given mass flow rate and pressure ratio as well as the stagnation pressure and temperature. The final equation used can be seen below.

$$A = \frac{\dot{m}}{\frac{P_o}{RT_o}\left(\frac{P_1}{P_{t1}}\right)^{\frac{1}{\gamma}}\sqrt{2c_p T_o}\sqrt{1 - \left(\frac{P_1}{P_{t1}}\right)^{\frac{\gamma-1}{\gamma}}}}$$

This equation was used in an excel spreadsheet to easily calculate and then plot the resulting bell mouth diameters, and the results are detailed in Chapter III.

THIS PAGE INTENTIONALLY LEFT BLANK

APPENDIX E. MACHINED BELL MOUTH ATTACHMENT DRAWINGS

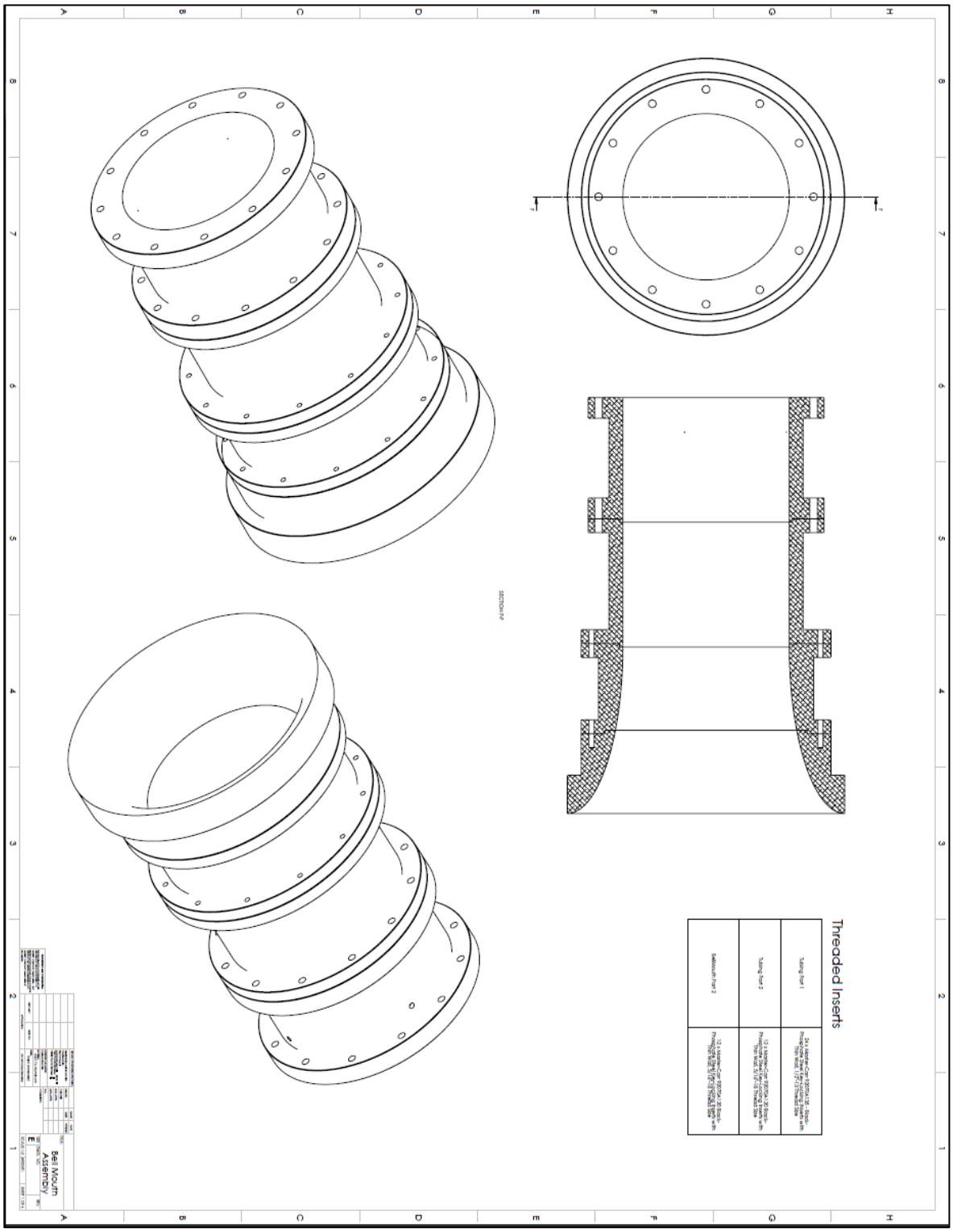

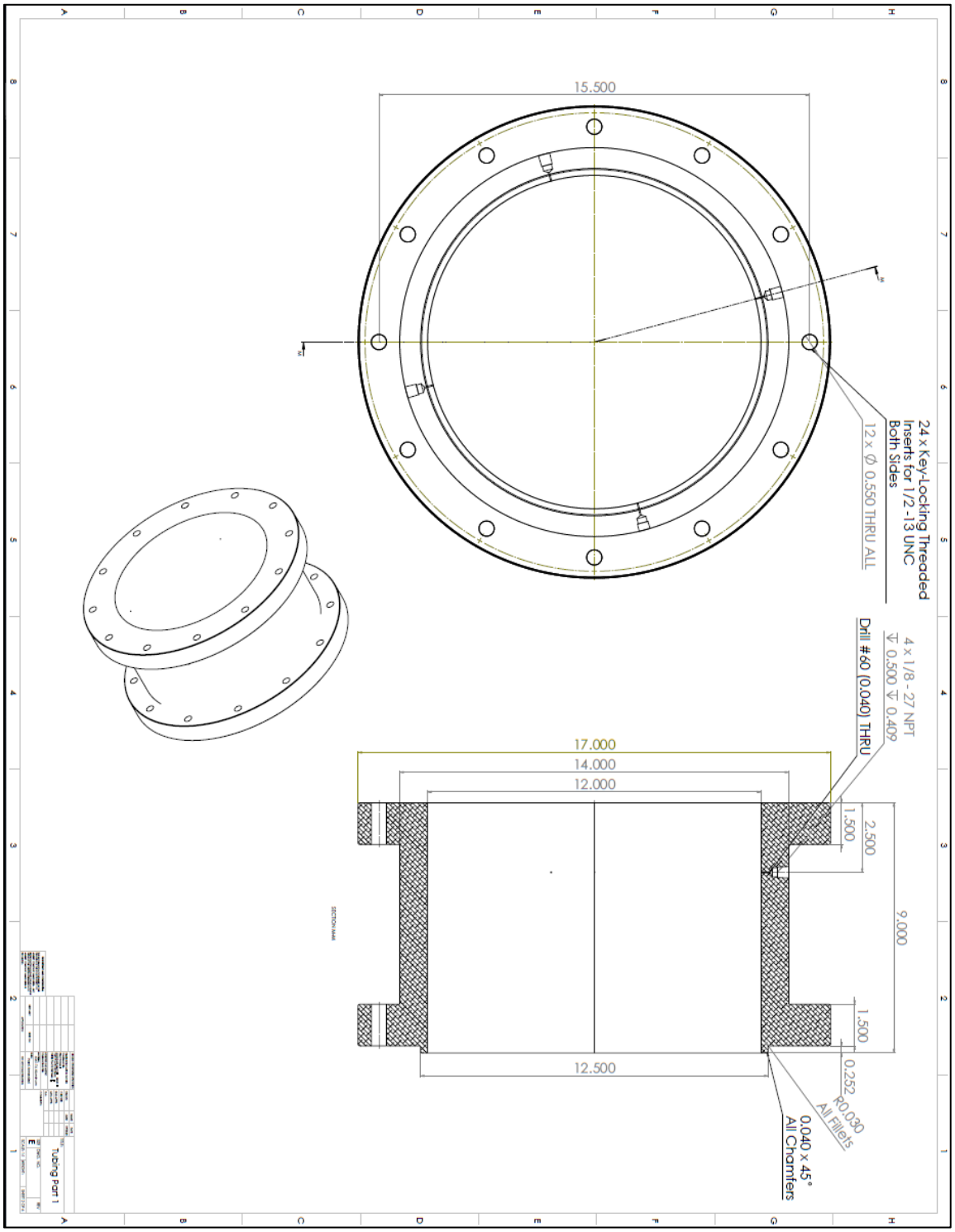
24 x Key-Locking Threaded
Inserts for 1/2 -13 UNC
Both Sides
12 x ∅ 0.550 THRU ALL
15.500
4 x 1/8 - 27 NPT
↧ 0.500 ↧ 0.409
Drill #60 (0.040) THRU
17.000
14.000
12.000
2.500
1.500
9.000
1.500
0.252
R0.030
All Fillets
0.040 x 45°
All Chamfers
12.500
SECTION A-A
Tubing Part 1

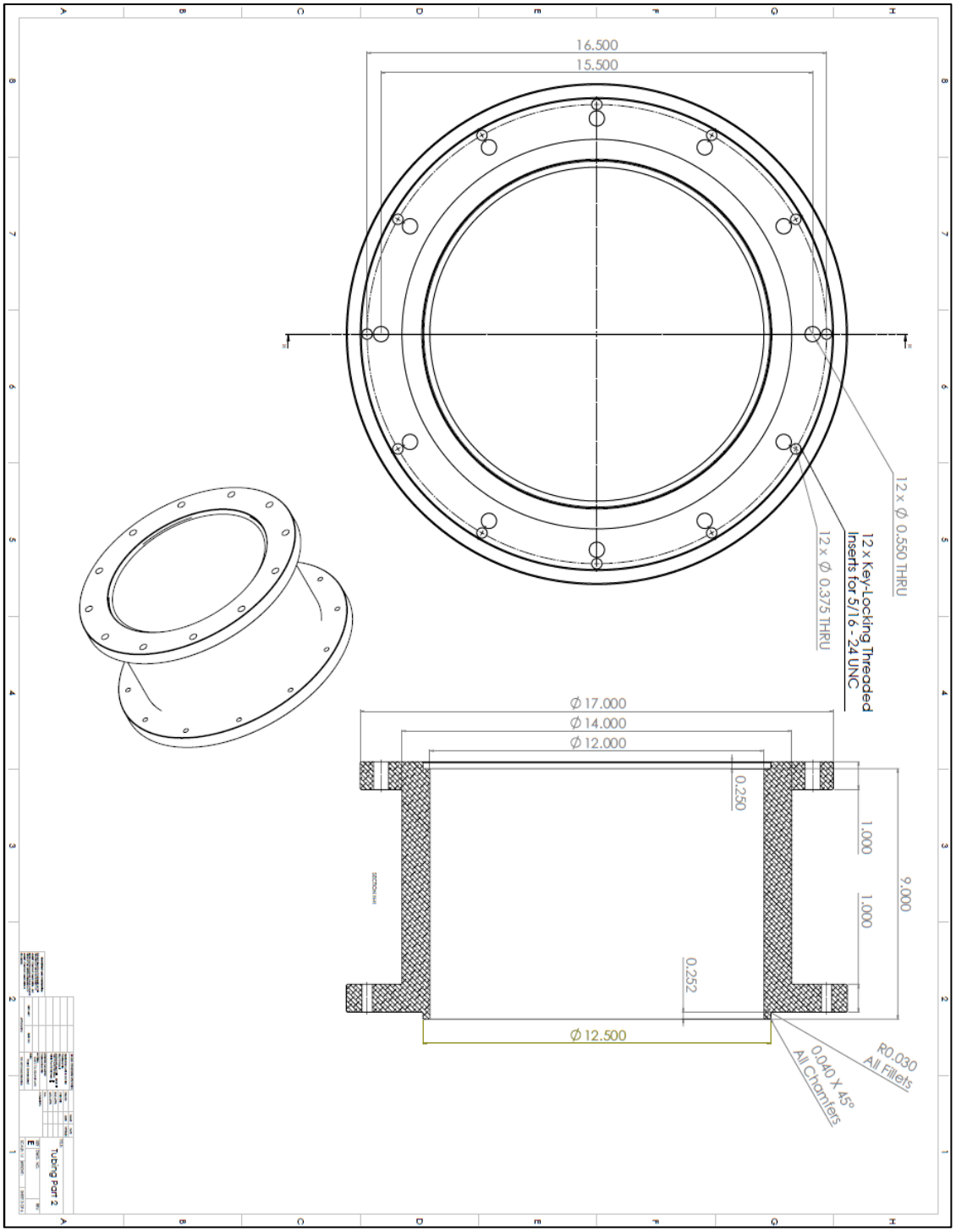
16.500
15.500
12 x Ø 0.550 THRU
12 x Key-Locking Threaded
Inserts for 5/16 - 24 UNC
12 x Ø 0.375 THRU
Ø 17.000
Ø 14.000
Ø 12.000
0.250
1.000
1.000
9.000
0.252
Ø 12.500
R0.030
All Fillets
0.040 X 45°
All Chamfers
Tubing Part 2

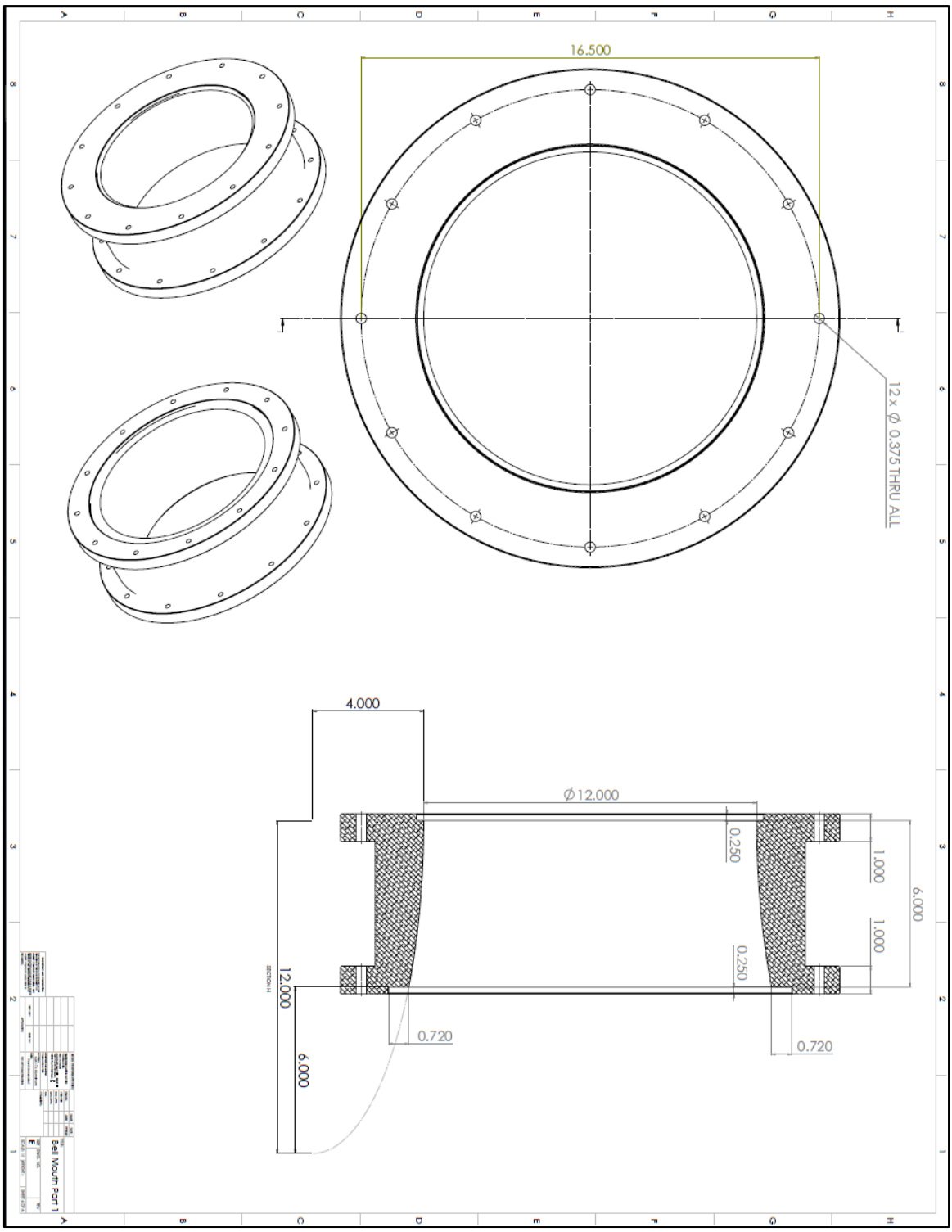
16.500
12 x ∅ 0.375 THRU ALL
4.000
∅12.000
0.250
1.000
6.000
1.000
0.250
12.000
0.720
6.000
0.720
Bell Mouth Part 1

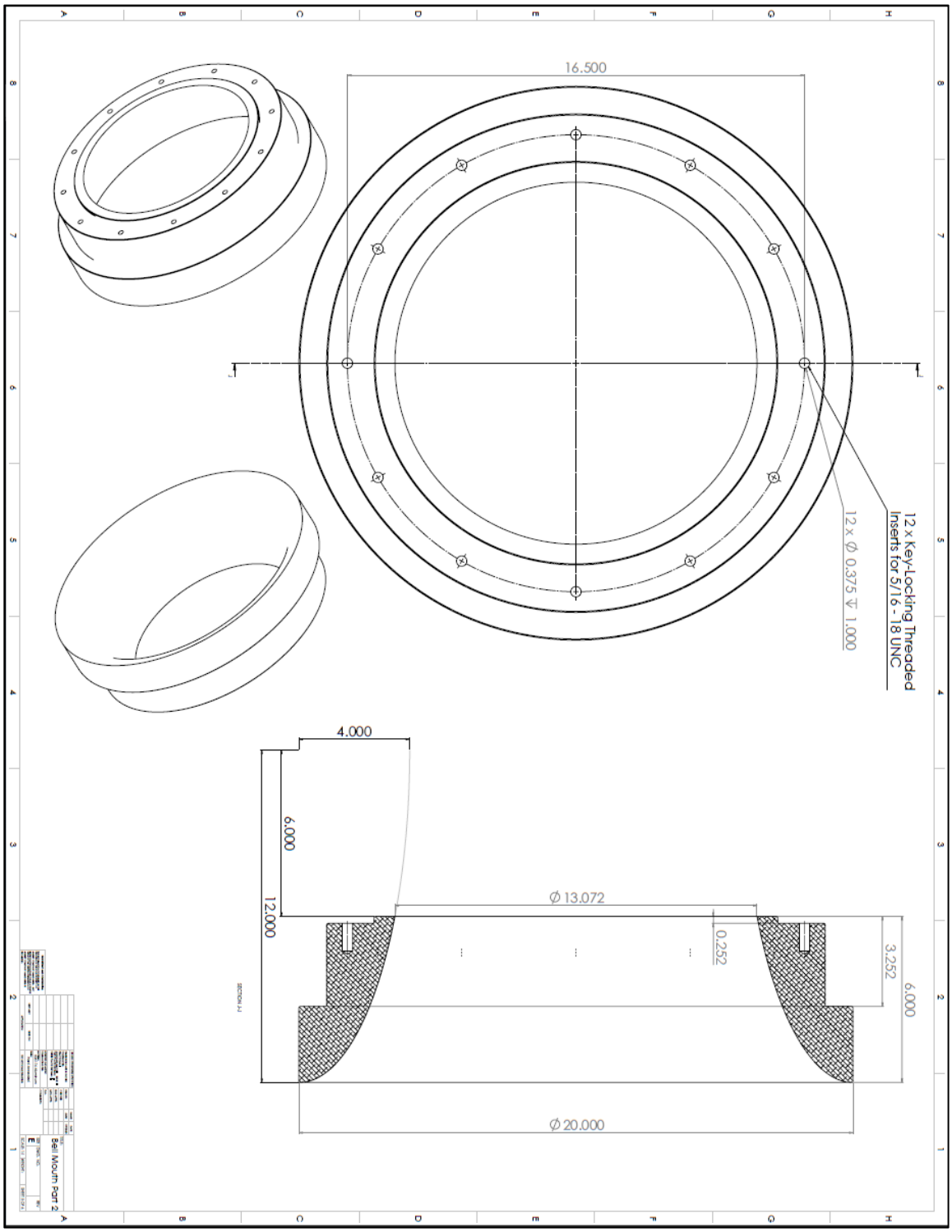
16.500
12 x Key-Locking Threaded
Inserts for 5/16 - 18 UNC
12 x ⌀ 0.375 ↧ 1.000
4.000
6.000
12.000
⌀ 13.072
0.252
3.252
6.000
⌀ 20.000
Bell Mouth Part 2

THIS PAGE INTENTIONALLY LEFT BLANK

APPENDIX F. CFX MODEL MESH STATISTICS

Global Mesh

Display	
Display Style	Use Geometry Setting
Defaults	
Physics Preference	CFD
Solver Preference	CFX
Element Order	Linear
Element Size	1.e-002 m
Sizing	
Use Adaptive Sizi...	No
Growth Rate	Default (1.2)
Max Size	Default (2.e-002 m)
Mesh Defeaturing	Yes
Defeature Size	Default (5.e-005 m)
Capture Curvature	Yes
Curvature Mi...	Default (1.e-004 m)
Curvature Nor...	10.0°
Capture Proximity	No
Bounding Box Di...	8.3061 m
Average Surface ...	0.18306 m^2
Minimum Edge L...	2.5357e-003 m
Quality	
Inflation	
Advanced	
Statistics	
Nodes	2576986
Elements	8135034

Sizings

Details of "Nozzle Inflation" - Inflation

Scope	
Scoping Method	Geometry Selection
Geometry	1 Body
Definition	
Suppressed	No
Boundary Scoping Method	Geometry Selection
Boundary	4 Faces
Inflation Option	First Layer Thickness
First Layer Height	2.e-005 m
Maximum Layers	10
Growth Rate	1.2
Inflation Algorithm	Pre

Details of "Wall Face Sizing" - Sizing

Scope	
Scoping Method	Geometry Selection
Geometry	9 Faces
Definition	
Suppressed	No
Type	Element Size
Element Size	5.e-003 m
Advanced	
Defeature Size	Default (5.e-005 m)
Behavior	Soft
Growth Rate	Default (1.2)
Capture Curvature	No
Capture Proximity	No

Details of "Throttle Face Sizing" - Sizing

Scope	
Scoping Method	Geometry Selection
Geometry	8 Faces
Definition	
Suppressed	No
Type	Element Size
Element Size	5.e-003 m
Advanced	
Defeature Size	Default (5.e-005 m)
Behavior	Soft
Growth Rate	Default (1.2)
Capture Curvature	No
Capture Proximity	No

Details of "Wall Inflation" - Inflation

Scope	
Scoping Method	Geometry Selection
Geometry	1 Body
Definition	
Suppressed	No
Boundary Scoping Method	Geometry Selection
Boundary	8 Faces
Inflation Option	First Layer Thickness
First Layer Height	1.e-004 m
Maximum Layers	10
Growth Rate	1.2
Inflation Algorithm	Pre

Details of "Nozzle Face Sizing" - Sizing

Scope	
Scoping Method	Geometry Selection
Geometry	4 Faces
Definition	
Suppressed	No
Type	Element Size
Element Size	1.e-003 m
Advanced	
Defeature Size	Default (5.e-005 m)
Behavior	Soft
Growth Rate	Default (1.2)
Capture Curvature	No
Capture Proximity	No

Details of "Throttle Inflation" - Inflation

Scope	
Scoping Method	Geometry Selection
Geometry	2 Bodies
Definition	
Suppressed	No
Boundary Scoping Method	Geometry Selection
Boundary	8 Faces
Inflation Option	First Layer Thickness
First Layer Height	1.e-004 m
Maximum Layers	10
Growth Rate	1.2
Inflation Algorithm	Pre

THIS PAGE INTENTIONALLY LEFT BLANK

APPENDIX G. KEY CFD SIMULATION RESULTS

Throttle Rotation (degrees)	Pressure Ratio	Mass Flow Rate (kg/s)	Max Mach Number
0	1.0100	0.38155	0.09525
0	1.0519	0.84426	0.21292
0	1.1095	1.1695	0.31551
0	1.1738	1.448	0.42677
0	1.2459	1.721	0.53124
0	1.3275	1.985	0.64209
5.996	1.0100	0.36481	0.09934
5.996	1.0519	0.81855	0.21720
5.996	1.1095	1.1373	0.30683
5.996	1.1738	1.4390	0.43326
5.996	1.2459	1.7090	0.53621
5.996	1.3275	1.9720	0.64686
12.273	1.0100	0.29384	0.11926
12.273	1.0519	0.64753	0.2662
12.273	1.1095	0.90773	0.38101
12.273	1.1738	1.1460	0.48629
12.273	1.2459	1.3620	0.5866
12.273	1.3275	1.5710	0.67902
14.956	1.0100	0.24507	0.12453
14.956	1.0519	0.53924	0.28064
14.956	1.1095	0.74595	0.40003
14.956	1.1738	0.9400	0.49015
14.956	1.2459	1.1170	0.59435
14.956	1.3275	1.2880	0.69803

THIS PAGE INTENTIONALLY LEFT BLANK

APPENDIX H. PERFORMANCE CURVES FOR NPSMF

80% Speed Data

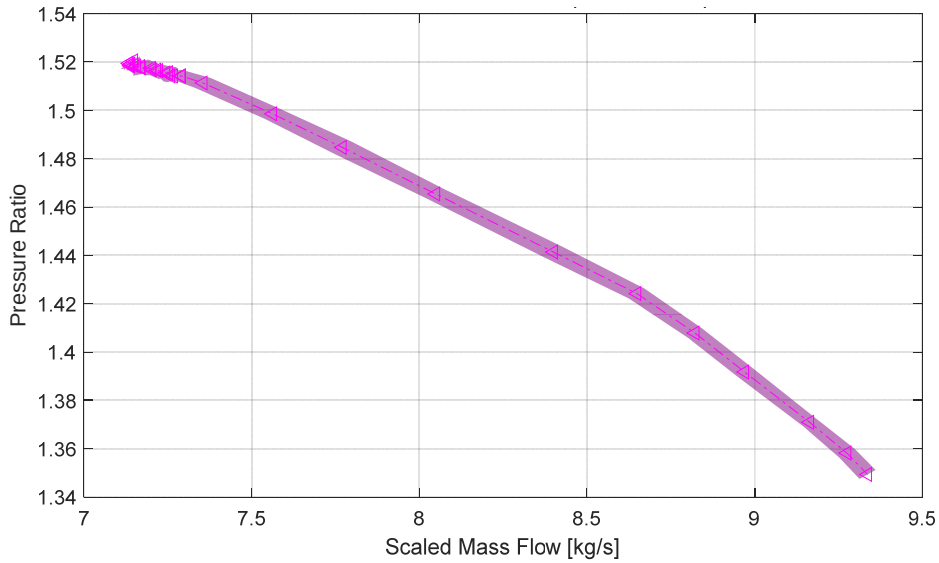

85% Speed Data

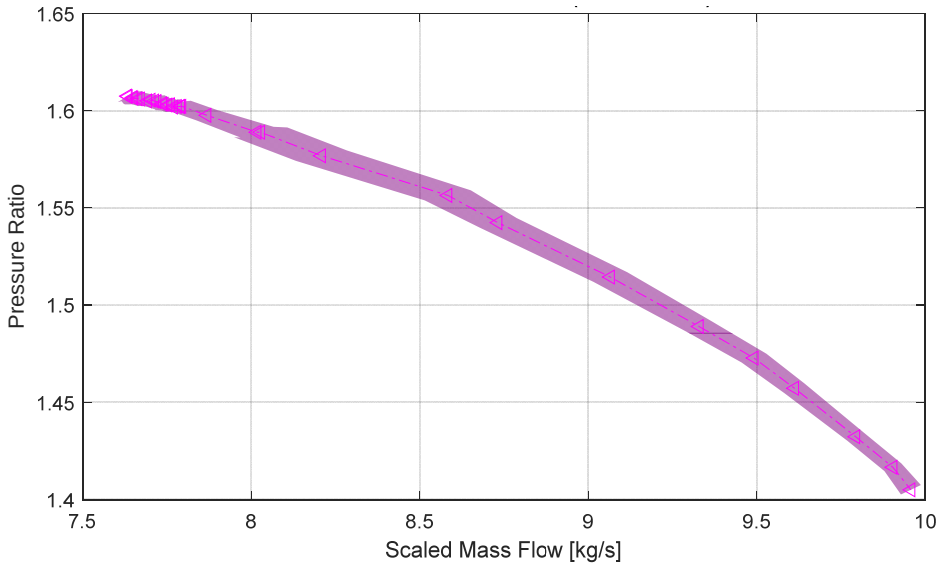

90% Speed Data

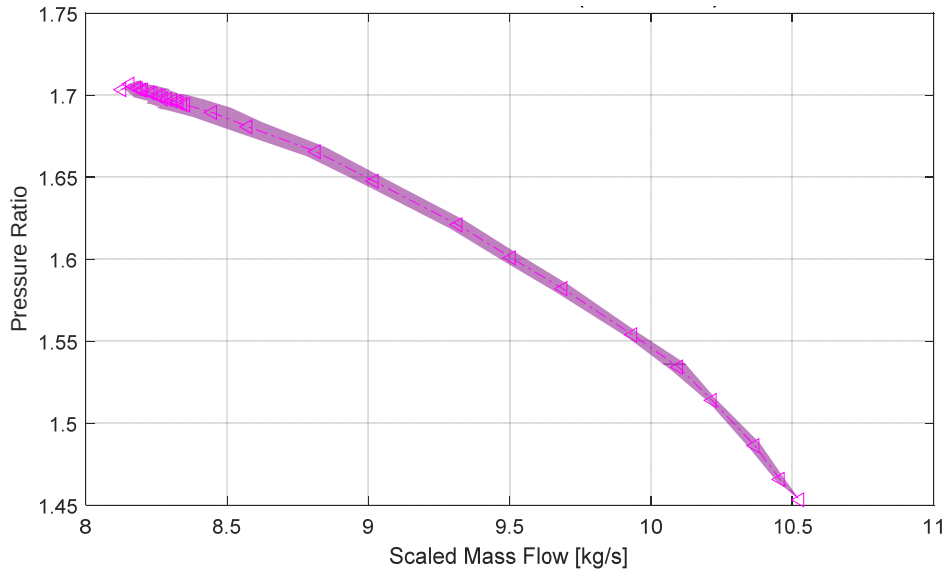

APPENDIX I. MASS-AVERAGED EFFICIENCY CURVES FOR NPSMF

80% Speed Data

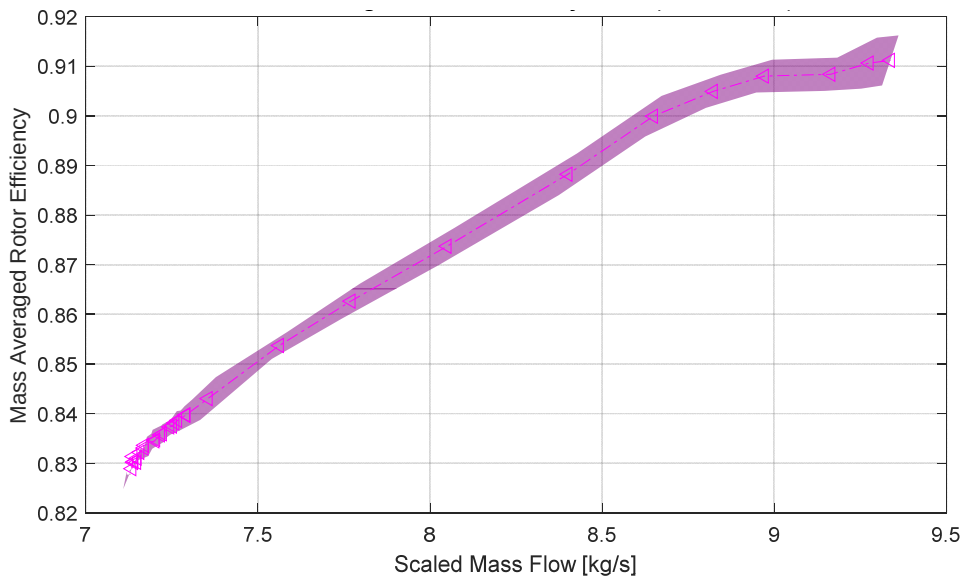

85% Speed Data

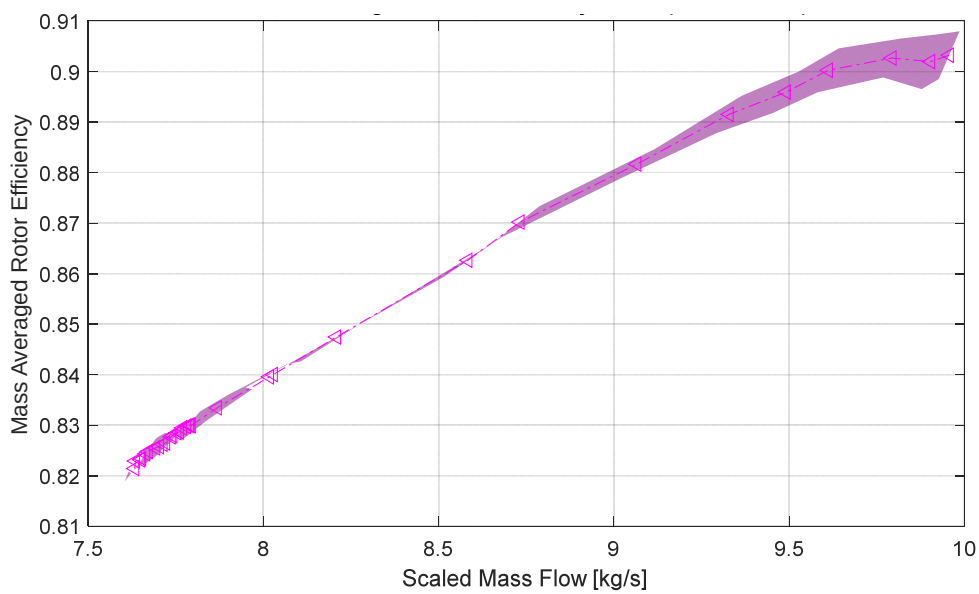

90% Speed Data

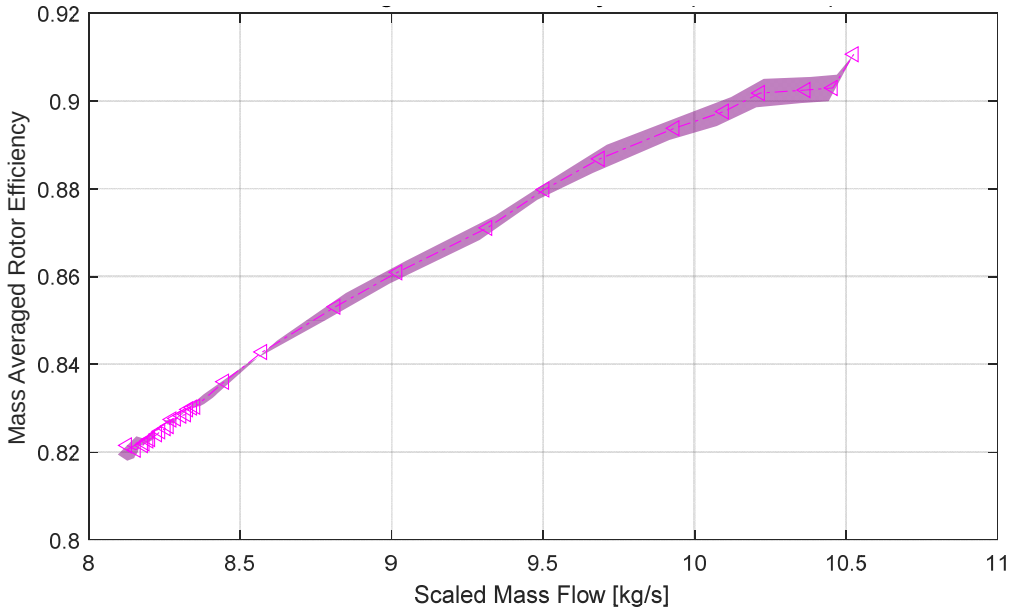

APPENDIX J. ADDITIONAL TCR AND BELL MOUTH ATTACHMENT VIEWS

Full Computational Domain of TCR with Current Box Inlet

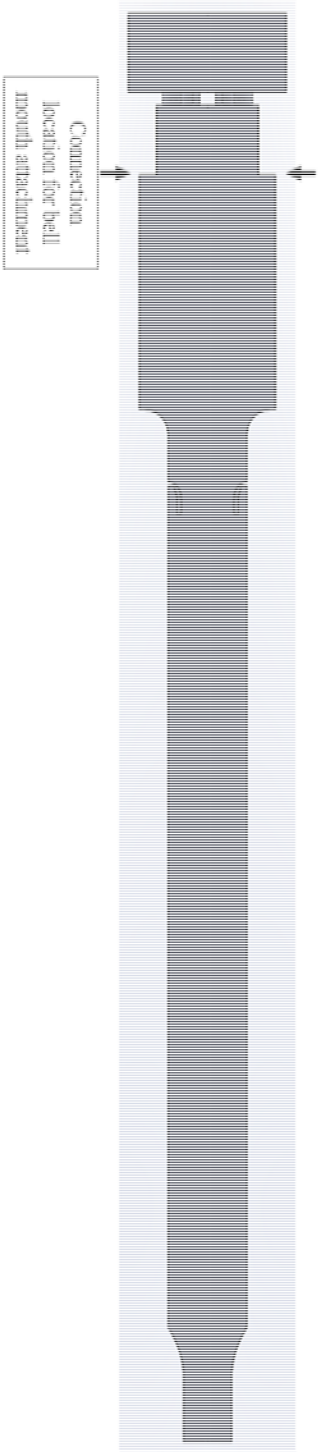

Assembly Drawing for Full Connected Bell Mouth Attachment

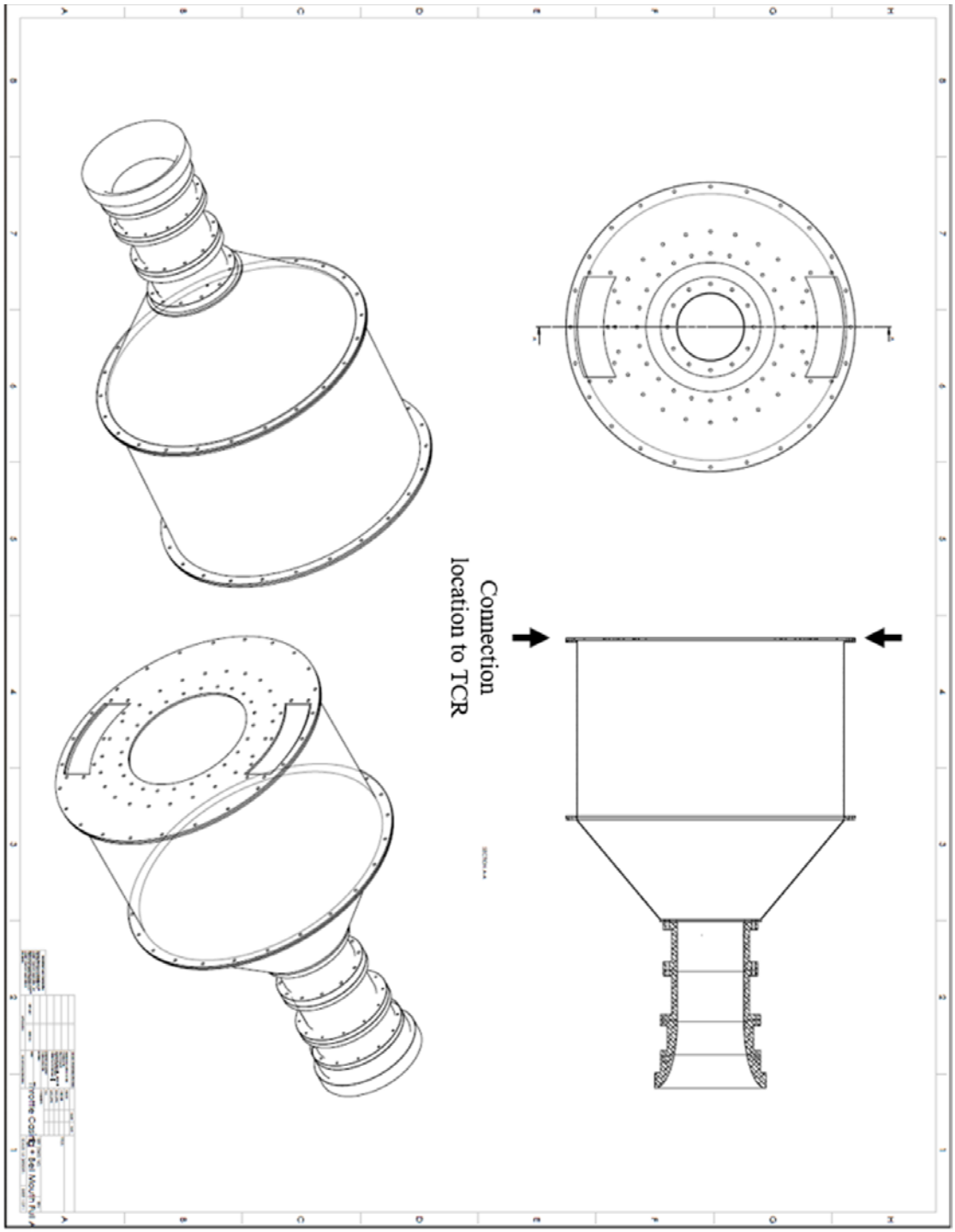

APPENDIX K. PRESSURE DROP ACROSS TCR COMPARISON

The following plot shows the pressure drop across the TCR drawn from the experimental data compared to the pressure drop data from a matched CFD simulation run. The matched run set the outlet static pressure equal to the outlet static pressure of this particular 70% speed test run, defined as “Ps1_avg” in the raw data file. The CFD matched simulation then set the inlet mass flow rate equal to the recorded, unscaled mass flow rate from the raw data, defined as “mdot_X” in the raw data file. The results of that simulation were then plotted on top of the experimental data, shown in Figure 38.

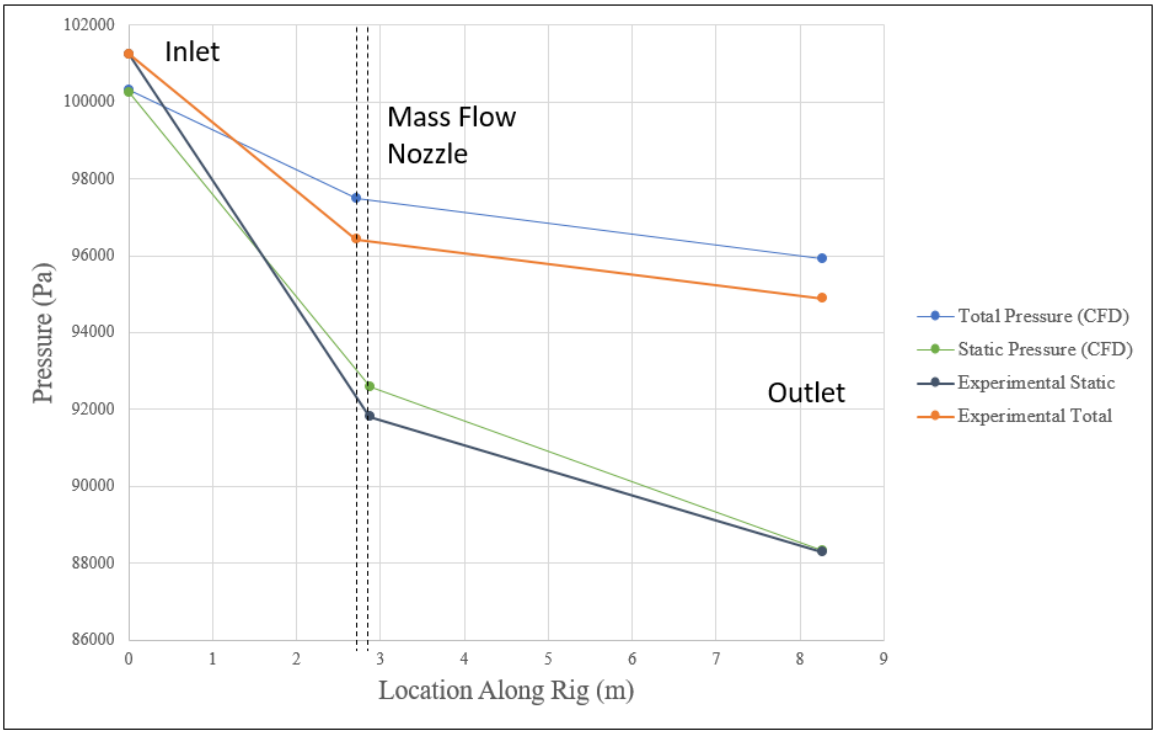

Figure 38. Pressure drop across the TCR for a matched 70% speed experimental test.

This plot shows that the slopes of dropping pressure from the flow nozzle to the outlet are very similar in the CFD and the experimental data. It also further shows that there is a greater pressure drop in the experimental data than the CFD simulation. This pressure

drop occurs between the inlet and the flow nozzle, more clearly linking it to the positioning of the flow straightening screens located within this section of the TCR.

SUPPLEMENTAL. EXPERIMENTAL RAW DATA FILE

The supplemental file shows the raw data recorded for each speed run of the NPSMF. This data was directly used for post processing and for the experimental analysis of the NPSMF shown in this thesis. It is available at the Dudley Knox Library at the Naval Postgraduate School.

THIS PAGE INTENTIONALLY LEFT BLANK

LIST OF REFERENCES

[1] Villescas, I. J., 2005, "Flow field surveys in a transonic compressor prior to inlet steam ingestion tests," M.S. thesis, MAE Department, Naval Postgraduate School, Monterey, CA, USA.

[2] Brunner, M. D., 2005, "Experimental and computational investigation of flow in a transonic compressor inlet," M.S. thesis, MAE Department, Naval Postgraduate School, Monterey, CA, USA.

[3] Payne, T. A., 2005, "Inlet flow-field measurements of a transonic compressor rotor prior to and during steam-induced rotating stall," M.S. thesis, MAE Department, Naval Postgraduate School, Monterey, CA, USA.

[4] Koessler, J. J., 2007, "Experimental investigation of high-pressure steam induced stall of a transonic rotor," M.S. thesis, MAE Department, Naval Postgraduate School, Monterey, CA, USA.

[5] Thorton, G. D., 2019, "Fluid-structure analysis of a transonic rotor," M.S. thesis, MAE Department, Naval Postgraduate School, Monterey, CA, USA.

[6] McNab, D. J., 2012, "Experimental testing and CFD modeling of an advanced transonic compressor for military applications," M.S. thesis, MAE Department, Naval Postgraduate School, Monterey, CA, USA.

[7] The American Society of Mechanical Engineers, 2011, "Measurement of Gas Flow by Bellmouth Inlet Flowmeters," MFC-26. New York, New York, USA.

[8] Blair, G. P., and W. M. Cahoon, "Best Bell," *Race Engine Technology*, September 2006. http://www.profblairandassociates.com/pdfs/RET_Bellmouth_Sept.pdf.

THIS PAGE INTENTIONALLY LEFT BLANK

INITIAL DISTRIBUTION LIST

1. Defense Technical Information Center
   Ft. Belvoir, Virginia

2. Dudley Knox Library
   Naval Postgraduate School
   Monterey, California